Bio- and chemostratigraphy of the Posidonia Shale: a new database for the Toarcian Oceanic Anoxic Event from northern Germany.

Stefano Visentin[a], Elisabetta Erba[a], Jörg Mutterlose[b]

[a]Dipartimento di Scienze della Terra, Università degli Studi di Milano, Via Mangiagalli 34, 20133 Milano, Italy (e-mails: stefano.visentin@unimi.it; elisabetta.erba@unimi.it)

[b]Institut für Geologie, Mineralogie und Geophysik, Ruhr-Universität Bochum, 44801 Bochum, Germany (e-mail: joerg.mutterlose@rub.de)

Corresponding author: Stefano Visentin (e-mail: stefano.visentin@unimi.it; tel.: (+39) 3293643336; Dipartimento di Scienze della Terra "Ardito Desio", Università degli Studi di Milano, Via Mangiagalli 34, 20133 Milano, Italy).

Abstract

We present calcareous nannofossil biostratigraphy, calcium carbonate and organic carbon isotope data of two cores drilled in the North German Basin (northern Germany) covering the upper part of the Amaltheenton-Formation (Fm) (upper Pliensbachian) and the Posidonienschiefer-Fm. (Toarcian). Fourteen bioevents spanning the latest Pliensbachian to late Toarcian time interval allowed the identification of the NJ5, NJ6 and NJ7 Zones of the Boreal biozonation.

The early Toarcian Oceanic Anoxic Event (T-OAE), identified by the organic carbon isotopic excursion within the Posidonienschiefer-Fm., is constrained by the first occurrences (FOs) of *Carinolithus superbus crassus* and *Diductius constans* at the onset of the $\delta^{13}C$ anomaly. The last occurrences (LOs) of the nannofossil species *Crepidolithus granulatus*, *Parhabdolithus liasicus distinctus*, *Biscutum finchii* and *Biscutum grande* are detected within the $\delta^{13}C$ isotopic anomaly. The new biostratigraphic data acquired in the North German Basin are compared to data from sections at higher and lower latitudes to evaluate event reproducibility relative to the $\delta^{13}C_{org}$ isotope curve. The FO of *C. superbus crassus* is an excellent datum to constrain the onset of the T-OAE at supraregional - global scale. Our finding indicates further nannofossil biohorizons within the T-OAE that might be useful at regional scale.

Keywords: Posidonia Shale, calcareous nannofossils, biostratigraphy, geochemistry, Toarcian Oceanic Anoxic Event, North German Basin.

1. Introduction

The Toarcian Posidonia Shale (Posidonienschiefer) has been in the focus of scientific research for more than 150 years (Röhl et al. 2001). Common findings of spectacular macrofossils have resulted in detailed descriptions of the marine fauna, which includes, among various groups of invertebrates, bony fish, sharks, ichthyosaurs, plesiosaurs, and marine crocodiles (e.g., Hauff 1960). Research has also dealt with sedimentological and geochemical issues (e.g., Seilacher 1970, Röhl et al. 2001). All large natural history museums have some of the extremely well-preserved specimens from this classical Fossillagerstätte on exhibition. According to the standard classification scheme of Fossillagerstätten (Seilacher 1970, Seilacher et al. 1985) the Posidonia Shale can be addressed as a Konservatlagerstätte.

Another aspect of the Posidonia Shale is its economic potential as a source rock for hydrocarbons (e.g., Demaison and Moore 1980, Frimmel et al. 2004). Studies on its geochemistry (Röhl et al. 2001, Schmid-Röhl et al. 2002) indicate an important negative excursion in $\delta^{13}C$ values in the lowermost part of the Posidonia Shale representing the expression of the early Toarcian Oceanic Anoxic Event (T-OAE) (Jenkyns 1988, 2010). This carbon (C) isotope anomaly, recorded in bulk rock, organic matter, fossil wood, carbonate microfraction and brachiopod calcite, is currently explained following two models. Küspert (1982) describes a scenario according to which dissolved inorganic carbon (DIC) is recycled from the deeper layers of a stratified water column (see also Saelen et al. 1996, Schouten et al. 2000, van de Schootbrugge et al. 2005). A second model implies methane release into the atmosphere/hydrosphere system and its subsequent oxidation to isotopically light CO_2 (e.g., Hesselbo et al. 2000, Jenkyns et al. 2002, McElwain et al. 2005, Kemp et al. 2005). Despite these intensive research activities, which are mainly aiming at developing a consistent depositional model, biostratigraphic studies across the Posidonia Shale remain scarce and mainly limited to ammonite stratigraphies. In particular, calcareous nannofossil investigations are sparse and almost completely restricted to the Dotternhausen and the Wittnau clay pit sections, for the Lower Toarcian and the Toarcian/Aalenian transition intervals respectively, both located in southern Germany (de Kaenel and Bergen 1996, Baldanza et al. 1996, Mattioli et al. 2004a, 2008, 2009). Recently, van de Schootbrugge et al. (2019) published the calcareous nannofossil biostratigraphy for the Schandelah Core, located in northern Germany. These authors published a precise and complete nannofossil biostratigraphic study from the Rhaetian to the Toarcian, including the Posidonianschiefer-Fm and providing both main and secondary events, which helped to constrain the boundaries between the calcareous nannofossil Zones. Nevertheless, the sample density adopted for the

Toarcian is relatively low being the investigated geological interval extremely wide. Therefore, a more exhaustive analysis focused on the Toarcian Posidonienschiefer-Fm of the Schandelah Core is required.

Based on material from two cores (L1, Schandelah) both drilled in the North German Basin, this paper has the following aims:

a) To provide a robust calcareous nannofossil biostratigraphic framework for the Toarcian Posidonia Shale of northern Germany.

b) To test the stratigraphic validity of specific biohorizons by comparing them with the standard biozonation scheme of the Boreal Realm (Bown and Cooper 1998).

c) To evaluate whether nannofossil events recognized prior, during and after the T-OAE isotopic anomaly display a supraregional signal or whether they are rather restricted to specific areas only (e.g., higher latitudes).

2. Geological setting

The North German Basin (NGB), a passive-active rift basin located in central and west Europe, represents one of the largest subbasins of the Central European Basin System (CEBS) and flanks the Ringkobing Fyn High to the north and the London-Brabant, the Rhenish and Bohemian Massifs to the south.

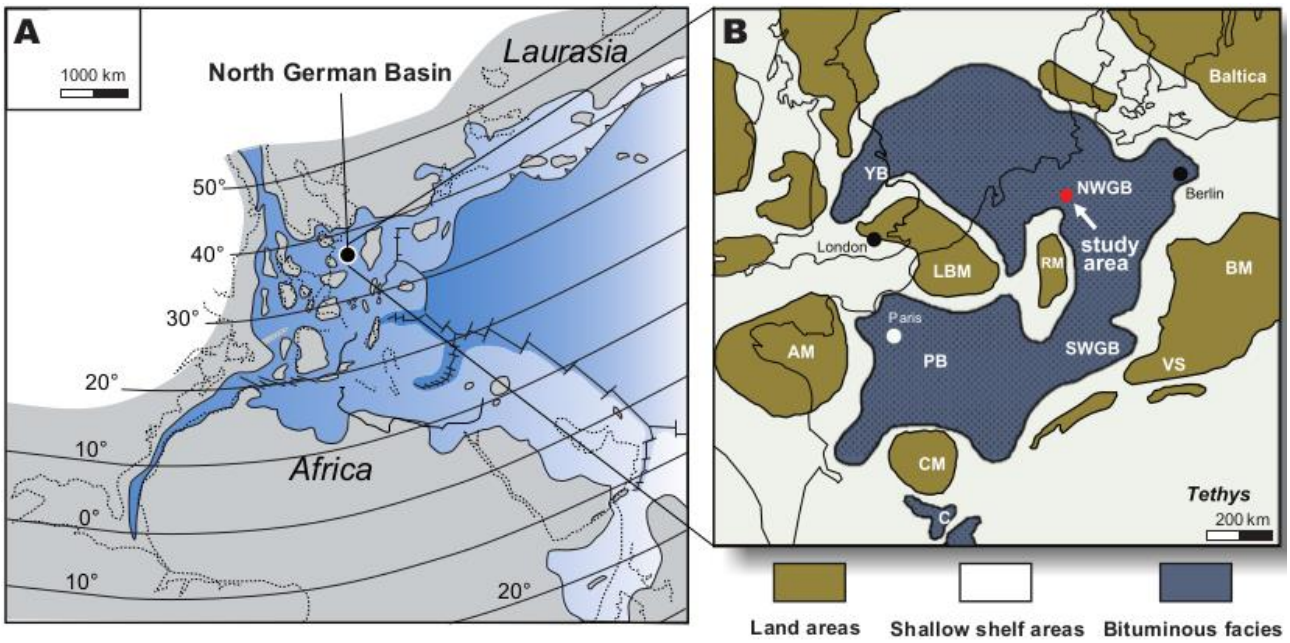

Fig. 1

The NGB was initiated during the Permo-Carboniferous by rifting of the litosphere subsequent to Variscan shortening (Ziegler 1990, Senglaub et al. 2006, Doornenbal and Stevenson 2010) and was accompanied by widespread volcanic activity followed by strong thermal subsidence in Permo-Triassic times, when continental siliciclastic sediments of the Rotliegendes as well as evaporites and limestones of the Zechstein were deposited

in the basin centre (Scheck and Bayer 1999, Kockel 2002, Kossow and Krawczyk 2002, Scheck-Wenderoth et al. 2008).

From the Triassic onward, the basin evolution was additionally influenced by salt mobilization and the Late Triassic – Jurassic extension principally controlled the structure of the E-W profile. The Triassic succession was characterized by rapidly deposited red-bed clastic sequences of the Buntsandstein overlain by Muschelkalk platform carbonates and the consequent lowering of the sea level in the Late Triassic led to renewed terrestrial sedimentation (Kossow and Krawczyk 2002).

During the Early Jurassic, present-day Europe was located on the broad and extensive Laurussian continental shelf that opened towards the southeast into the Tethys Ocean (Ziegler 1982). The shelf area contained numerous deeper sub-basins separated by various submarine sills and islands of variable size (Fig. 1.a). All these structural features contributed to episodic restrictions of water circulation across the shallow shelf, especially during periods of sea level lowstand (Frimmel et al. 2004). The early Toarcian was characterized by an extensive transgressive phase, associated with the breakup of Pangea (Haq et al. 1988, Hallam 2001) which led to the deposition of organich-rich mudrocks (black shales) across Europe. The lithological expression of black shales in the NGB is the Posidonia Shale (Posidonienschiefer in German) which is present throughout the entire NGB except for the westernmost part (Kockel et al. 1994). The study area in NW Germany was connected to other shelf sub-basins with bituminous black shale deposition. To the west, these basins included the Paris Basin, to the south, the South German Basin, and to the north, the Yorkshire Basin (Fig. 1.b).

3. Lithostratigraphy of cores L1 and Schandelah

The two cores investigated in the present work were drilled in the Hildesheim-Braunschweig area, close to the villages of Hildesheim (L1 Core) and Schandelah (Schandelah Core) in northern Germany (Fig. 2). Samples from the L1 Core were collected in the core shed of the Wintershall-Dea oil company in Wietze (Germany). The Schandelah Core was sampled in the core repository of the German Federal Institute of Geosciences and Natural Resources in Berlin Spandau.

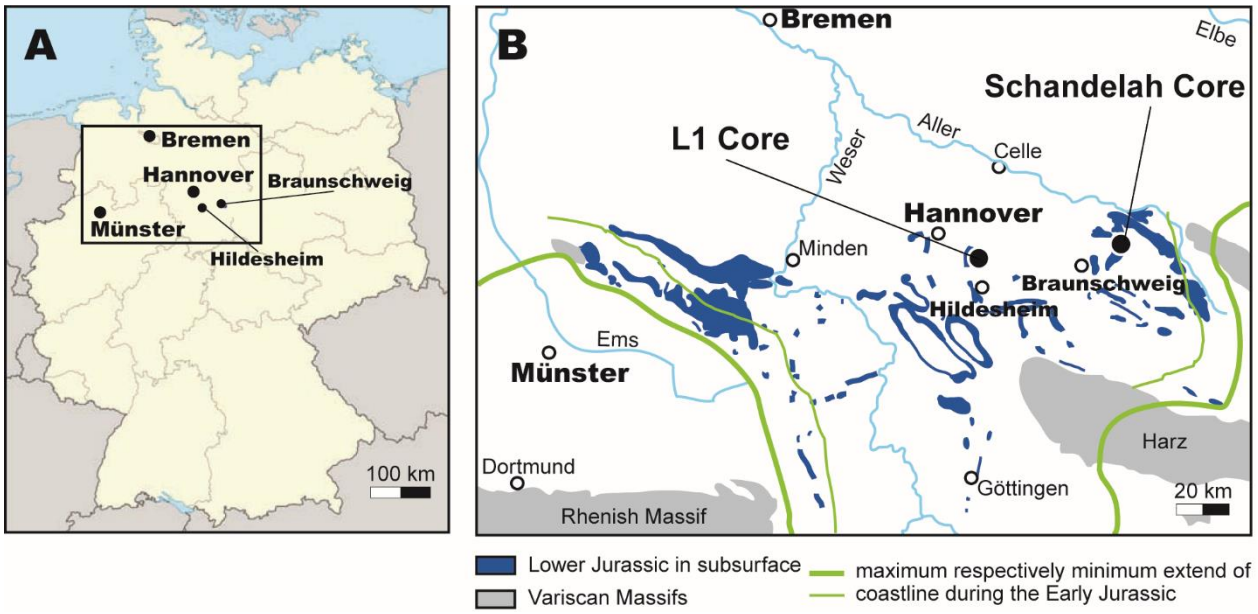

Fig. 2

Lithostratigraphy of the L1 and Schandelah cores are reported in Figs. 3 and 4, respectively. The 16 m-thick studied interval of the L1 Core spans the upper Amaltheenton-Fm and the lower Posidonienschiefer-Fm. The 46.5-m-thick interval of the Schandelah Core includes the upper Amaltheenton-Fm and the entire Posidonienschiefer-Fm.

A total of five lithostratigraphic units are recognized and described from the bottom to the top. Unit 5 (Amaltheenton-Fm.) is represented by medium grey claystone with silty to sandy light brownish grey strings. Unit 4 corresponds to the lowermost part of the Posidonienschiefer-Fm. This unit differs clearly from the overlying units 3, 2 and 1 of the Posidonienschiefer as it is strongly bioturbated and still consists of claystone (dark and greenish grey) with silty to sandy strings. Unit 4 in the L1 Core is less bioturbated compared to that of Schandelah Core and appears correlative of unit 5. Moreover, two isolated concretionary layers are detected within this unit, namely, at 46 m and 43 m (Schandelah Core) and at 27.6 m and 26.4 m (L1 Core). Based on literature survey these concretionary layers possibly refer to “Siemensi” and “Capillatum” concretions, respectively. Following van de Schootbrugge et al. (2019) the Pliensbachian/Toarcian boundary is placed between Units 5 and 4, at 48 m in the Schandelah Core. It is not possible to clearly identify the Pliensbachian/Toarcian boundary in the L1 Core as a reliable boundary between units 5 and 4 was not observed. Units 3, 2 and 1 are represented by the Posidonienschiefer style facies, i.e., paper shales. Unit 3 is constituted by dark grey, dark brown and black bituminous marly claystone and fissile black shales with two isolated concretionary layers. Those are detected exclusively in the L1 Core, at 24.4 m and 24 m and possibly

refer to the “Elegantulum” and “Boreale” concretions, respectively. The transition between the bioturbated claystone and the laminated marly claystone appears sharp in the L1 Core and more gradual in the Schandelah Core, supporting the presence of a hiatus at the base of unit 3 in the L1 Core (Fig. 3). Unit 2 is constituted by medium brown bituminous marlstone with light grey carbonate beds and concretionary layers. Among the carbonate beds, the “Elegans Bank” is recognized from 40 to 39.25 m in the Schandelah Core and from 22 to 21.25 m in the L1 Core. The “Monotis Bank” is present from 31.75 to 31.25 m in the Schandelah Core and from 15.15 m to top in the L1 Core. This regional marker bed is characterized by a peculiar wavy lamination and a conspicuous shell accumulation mainly from left valves of the bivalve *Meleagrinella substriata* and local accumulations of the ammonite *Dactylioceras athleticum* (Arp and Gropengießer 2016). An additional carbonate bed is found in both cores between 35.1 and 34.6 m in the Schandelah Core and from 18 to 17.5 m in the L1 Core. A further concretionary layer is detected at 33.5 m and at 16.77 m in the Schandelah and L1 cores, respectively.

The onset and the termination of the T-OAE are placed in accordance with the $\delta^{13}C_{org}$ stable isotope excursion, recorded as a synchronous signal worldwide, namely, from 24.9 to 22 m in the L1 Core and from 43 to 40 m in the Schandelah Core, thus spanning the uppermost unit 4 (only in Schandelah Core), the whole unit 3 and the lowermost unit 2 up to the base of the “Elegans Bank” in both cores.

Unit 1, recovered exclusively in the Schandelah Core, represents an undisturbed sequence of medium brown bituminous marly claystone without carbonate beds or concretionary layers. Ammonite stratigraphy is provided according to the studies of Hoffmann (1968) and Weitschat (1973).

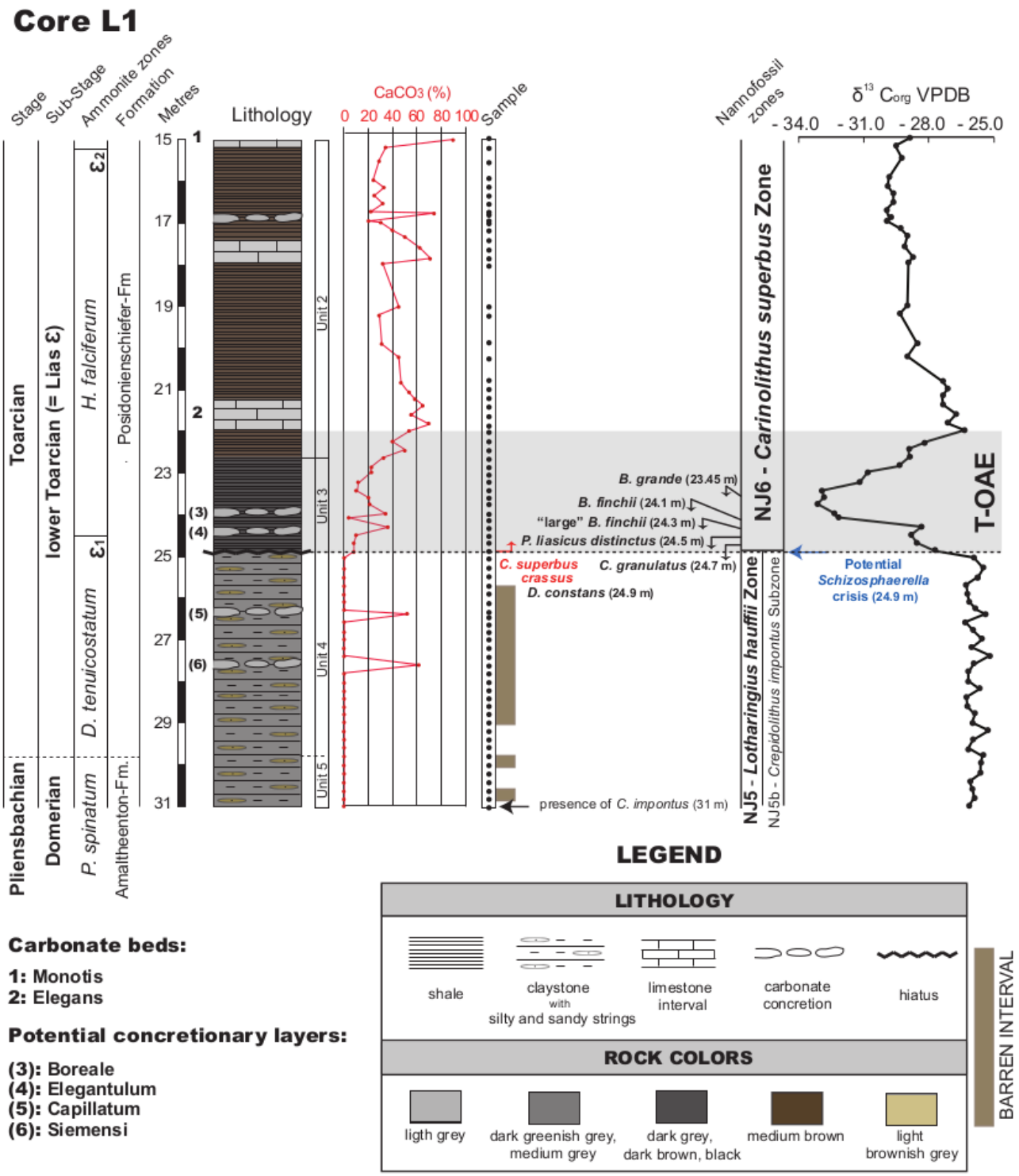
Core L1
Stage
Sub-Stage
Ammonite zones
Formation
Metres
Lithology
CaCO3 (%)
0 20 40 60 80 100
Sample
Nannofossil zones
δ13 Corg VPDB
- 34.0 - 31.0 - 28.0 - 25.0
Toarcian
lower Toarcian (= Lias ε)
Pliensbachian
Domerian
P. spinatum
D. tenuicostatum
H. falciferum
ε1
ε2
Posidonienschiefer-Fm.
Amaltheenton-Fm.
15
17
19
21
23
25
27
29
31
1
2
(3)
(4)
(5)
(6)
Unit 2
Unit 3
Unit 4
Unit 5
B. grande (23.45 m)
B. finchii (24.1 m)
"large" B. finchii (24.3 m)
P. liasicus distinctus (24.5 m)
C. superbus crassus
C. granulatus (24.7 m)
D. constans (24.9 m)
presence of C. impontus (31 m)
NJ6 - Carinolithus superbus Zone
NJ5 - Lotharingius hauffii Zone
NJ5b - Crepidolithus impontus Subzone
T-OAE
Potential Schizosphaerella crisis (24.9 m)
LEGEND
LITHOLOGY
shale
claystone with silty and sandy strings
limestone interval
carbonate concretion
hiatus
ROCK COLORS
ligth grey
dark greenish grey, medium grey
dark grey, dark brown, black
medium brown
light brownish grey
BARREN INTERVAL
Carbonate beds:
1: Monotis
2: Elegans
Potential concretionary layers:
(3): Boreale
(4): Elegantulum
(5): Capillatum
(6): Siemensi

139 Fig. 3

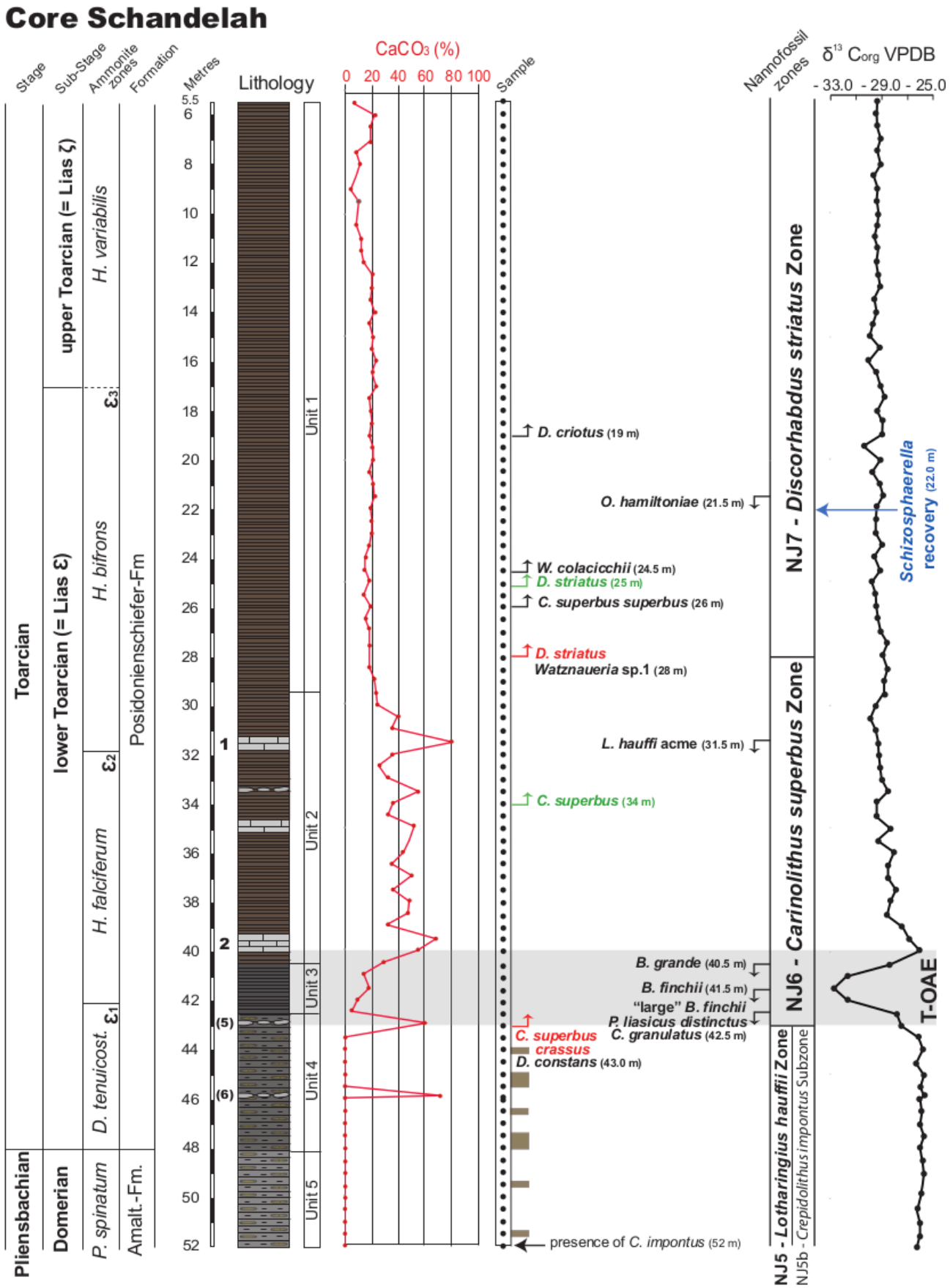

Fig. 4

4. Materials and methods

142 4.1. Biostratigraphy

143 Calcareous nannofossil biostratigraphy was performed on a total of 168 samples. Seventy-three samples were
144 studied from the upper Amaltheenton-Fm. and lower Posidonienschiefer-Fm. of the L1 Core (Fig. 3). Ninety-
145 five samples were investigated from the upper Amaltheenton-Fm. and Posidonienschiefer-Fm. of the
146 Schandelah Core (Fig. 4). The sampling resolution varies between one sample/20 cm to one sample/50 cm for
147 the L1 Core and one sample/50 cm for the Schandelah Core.

148 Simple smear slides of each sample were prepared following the method of Roth (1983): a small amount of
149 rock material was powdered adding few drops of bi-distillate water, without centrifuging, ultrasonic cleaning
150 or settling the sediment in order to retain the original composition. The obtained suspension was mounted onto
151 a slide, covered with a cover slide fixed with Norland Optical Adhesive. Each sample was examined for
152 calcareous nannofossils using a Leica DM 2700 P light polarizing microscope with a magnification of 1250X.
153 A total of 300 determinable nannofossil specimens were counted in each slide. Additional 1000 fields of view
154 for each smear slide were investigated to recognize rare and biostratigraphic important taxa. Several samples
155 belonging to the Amaltheenton-Fm. (Unit 5) and the lower portion of the Posidonienschiefer-Fm. (Unit 4) are
156 barren of nannofossils, others contain extremely rare specimens (less than 10 specimens in 1000 fields of view)
157 being these units strongly depleted in calcium carbonate content in both cores (Figs. 3, 4). In these samples the
158 300-specimen counting was not performed (Figs 5, 6). The preservation of calcareous nannofossils was
159 evaluated using the visual criteria of Roth and Thierstein (1972) and Roth (1983) for assessment of etching
160 (E) and overgrowth (O), with E1/O1 standing for minor, E2/O2 for moderate and E3/O3 for major
161 etching/overgrowth. We adopted the calcareous nannofossil biozonation scheme of Bown (1987) revised by
162 Bown et al. (1988) and Bown and Cooper (1998). Calcareous nannofossil taxa recognized are listed in
163 Appendix 1 and illustrated in Plates 1 and 2. The stratigraphic distribution of biostratigraphic index taxa and
164 their abundances are reported in Figs. 5 and 6.

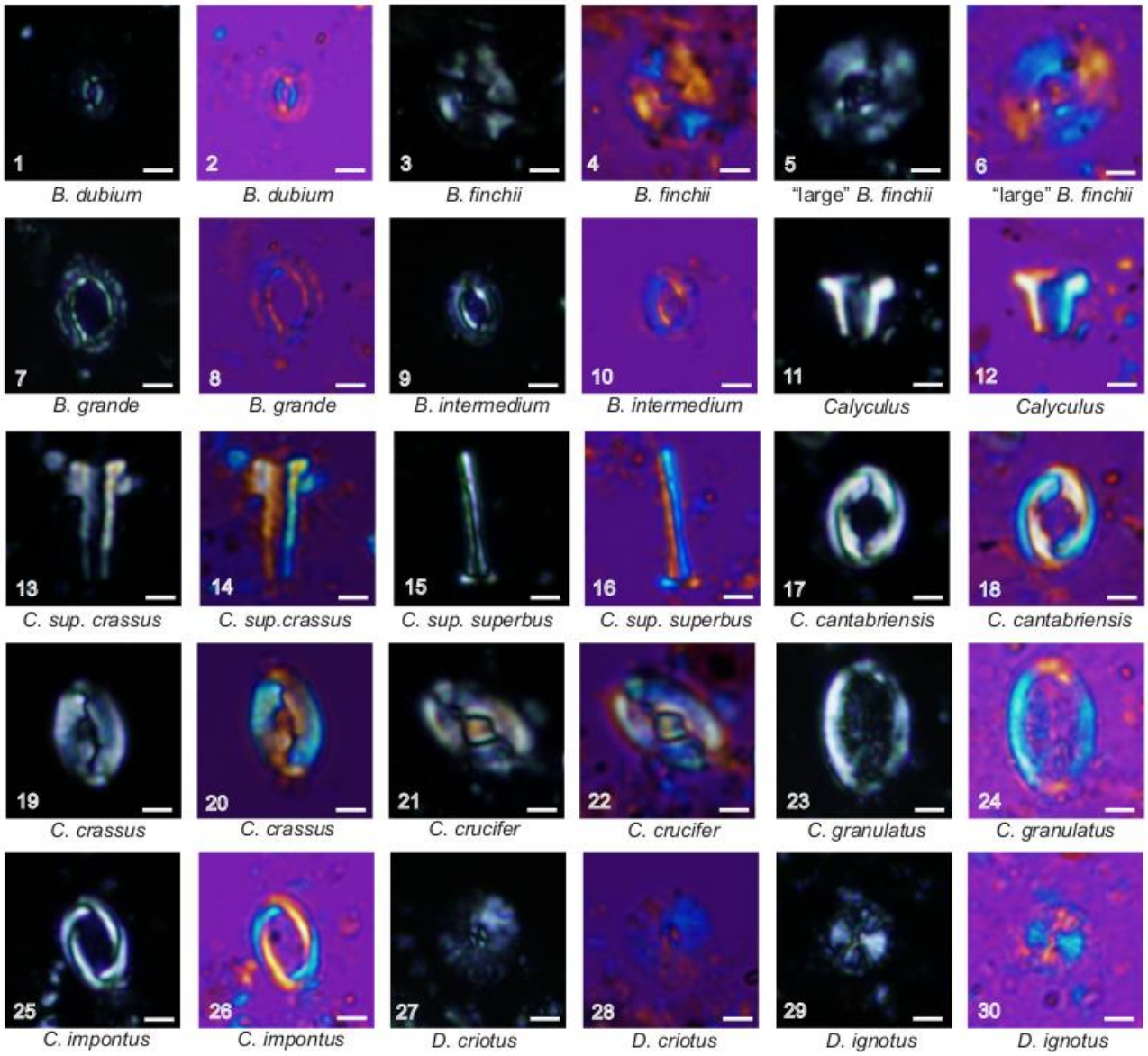
1 B. dubium
2 B. dubium
3 B. finchii
4 B. finchii
5 "large" B. finchii
6 "large" B. finchii
7 B. grande
8 B. grande
9 B. intermedium
10 B. intermedium
11 Calyculus
12 Calyculus
13 C. sup. crassus
14 C. sup.crassus
15 C. sup. superbus
16 C. sup. superbus
17 C. cantabriensis
18 C. cantabriensis
19 C. crassus
20 C. crassus
21 C. crucifer
22 C. crucifer
23 C. granulatus
24 C. granulatus
25 C. impontus
26 C. impontus
27 D. criotus
28 D. criotus
29 D. ignotus
30 D. ignotus

165 Plate 1

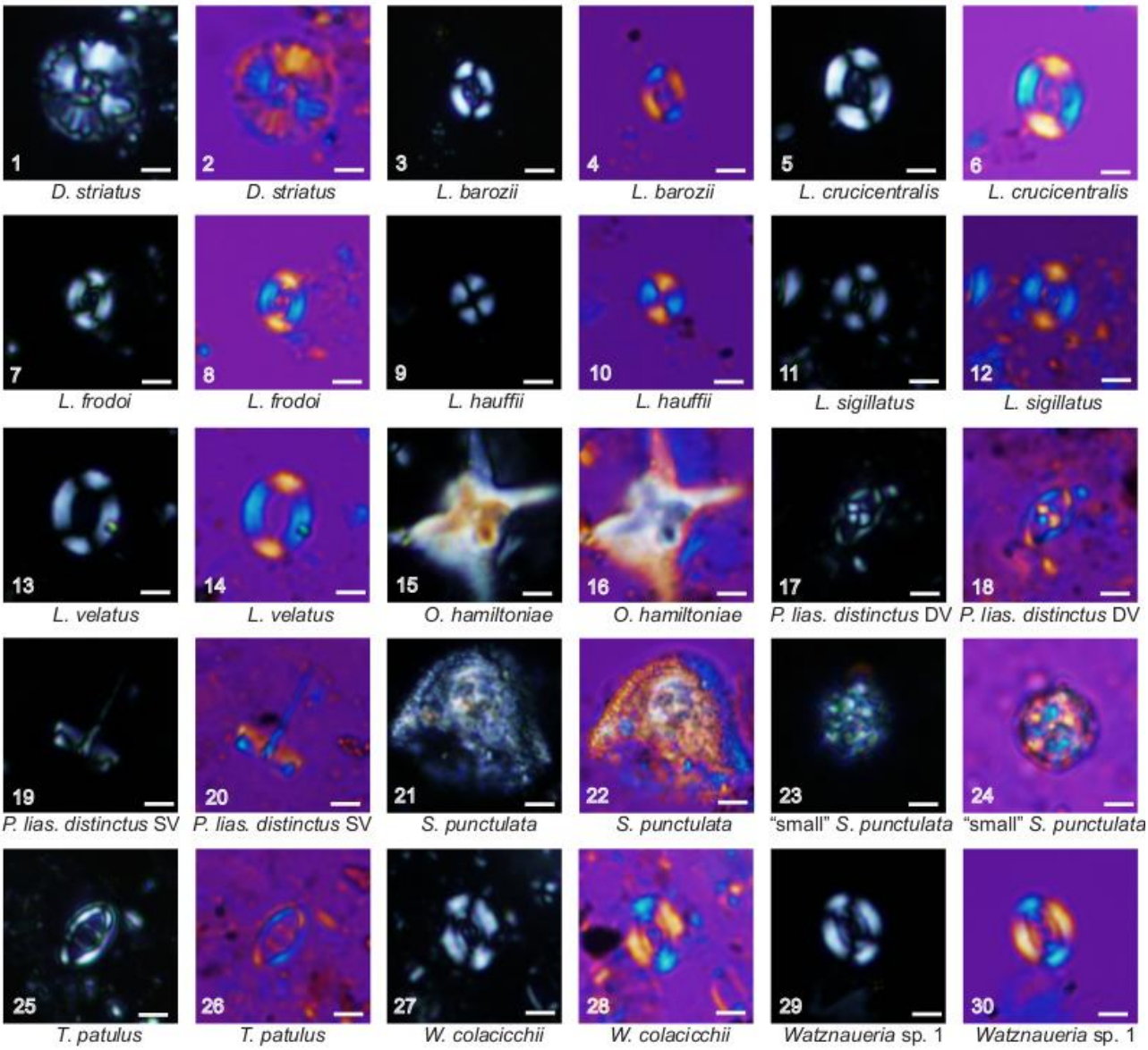

Plate 2

4.2. Geochemistry

Bulk rock subsamples of the same 168 samples selected for biostratigraphy were analysed for calcium carbonate content by using the "Karbonat-Bombe" (Müller and Gastner 1971) and carbon isotope analyses of organic carbon with a Flash EA 2000 elemental analyser connected online to ThermoFinnigan Delta V Plus mass spectrometer at the GeoZentrum Nordbayern, Friedrich-Alexander Universität Erlangen-Nürnberg. All carbon isotope values were calibrated to the V-PDB (Vienna-PDB) standard. Accuracy and reproducibility of the analyses were checked by replicate analyses of laboratory standards calibrated to international standards USGS 40 and 41. Calcium carbonate and organic carbon isotope curves of the two cores are reported in Figs. 3 and 4.

5. Taxonomic notes

This chapter reports observations concerning morphological and/or dimensional features of certain taxa (*Biscutum finchii*, *Carinolithus superbus*, *Schizosphaerella punctulata*), alphabetically ordered by genus, observed under the light polarizing microscope. In the studied cores, indeed, taxonomic peculiarities concerning these species were detected for the first time or consistently to recent published papers (i.e., Visentin et al. 2021), thus requiring a deeper discussion aimed at carrying out a precise and exhaustive biostratigraphy.

Genus *Biscutum* Black *in* Black and Barnes (1959)

Biscutum finchii (Crux 1984) Bown (1987)

Remarks. This species was introduced by Crux (1984) and subsequently emended by Bown (1987). De Kaenel and Bergen (1993) and Mattioli (2004b) proposed the inclusion of *B. finchii* in the genus *Similiscutum* because of the unicyclic distal shield structure. Cobianchi (1990, 1992) and Picotti and Cobianchi (1996) distinguished specimens characterized by a distal shield length < 6 µm as *B.* aff. *B. finchii* and "small" *B. finchii* respectively. Later, Casellato and Erba (2015) detected specimens smaller than the holotype (5.6 µm length – 4.7 µm width) with subcircular outline and prominent distal shield. These are grouped by the authors as "small" *B. finchii* similarly to previous authors. In our study "small" *B. finchii* as defined by Casellato and Erba (2015) were not detected. Specimens bigger than the maximum range proposed for *B. finchii* (7.0 µm length) have been found and addressed as "large" *B. finchii.* This morphotype possibly corresponds to *S. giganteum* observed by previous authors (e.g., Mailliot et al. 2006, Ferreira et al. 2015, da Rocha et al. 2016) and *S.* aff. *S. finchii* "large" (e.g., Kafousia et al. 2014, Menini et al. 2019).

Genus *Carinolithus* Prins *in* Grün et al. (1974)

Carinolithus superbus (Deflandre *in* Deflandre and Fert 1954) Prins *in* Grün et al. (1974)

Remarks. In the present work we follow the recent taxonomic revision for the genus *Carinolithus* proposed by Visentin et al. (2021). This work foresees a subdivision between *C. superbus crassus* and *C. superbus superbus* based on the stem width (SW). The former taxon has a SW > 1 µm whereas the latter ≤ 1 µm. Based on available data, Visentin et al. (2021) concluded that the FO of *C. superbus* used as marker for the base of the NJ6 and NJT6 Zone in the standard schemes (i.e., Bown 1987, Bown et al. 1988, Bown and Cooper 1998, Fraguas et al. 2015, 2018 for the NJ6; Mattioli and Erba, Ferreira et al. 2019 for the NJT6), is indeed the FO of *C. superbus crassus*. Thus, we use here the *C. superbus crassus* biohorizon. Visentin et al. (2021) further

205 shows that the species *C. cantaluppii* is a diagenetic artefact of the genus *Carinolithus* due to intensive
206 overgrowth (highly calcified *C. poulnabronei* and *C. superbus*) and, accordingly, in this work we disregard
207 this taxon.
208 Genus *Schizosphaerella* Deflandre and Dangeard (1938)
209 ***Schizosphaerella punctulata*** Deflandre and Dangeard (1938)
210 **Remarks**. This species was described by Deflandre and Dangeard (1938) as a nannolith composed by two
211 interlocked valves with a diameter of 12 – 30 µm. Later, Bown (1987) and Cobianchi (1992) reported a
212 diameter of 8 – 12 µm, whereas Mattioli and Pittet (2002) documented a size range of 7 – 13.5 µm. Casellato
213 and Erba (2015) separated specimens displaying dimensions of 4 – 7 µm as "small" *S. punctulata* from those
214 ≥ 7 µm (*S. punctulata*). Moreover, the same authors, observed additional specimens surrounded by a fringing
215 crust of radiating prismatic crystals grouped as "encrusted" *S. punctulata*, probably corresponding to over
216 calcified *Schizosphaerella* (Kälin 1980, Kälin and Bernoulli 1984). Encrusted *S. punctulata* specimens were
217 not detected in the investigated samples.
218 **6. Results**
219 6.1. Calcareous nannofossil preservation
220 For the few detected specimens in units 5 and 4, using the visual criteria of Roth and Thierstein (1972) and
221 Roth (1983), a moderate to moderate/good preservation was observed with minor/moderate etching (E1/2) and
222 negligible to minor overgrowth (O0 to O1). In some restricted intervals calcareous nannofossils are poorly
223 preserved and replaced by siderite showing yellowish colours, moderate etching (E2) and major overgrowth
224 (O3), (L1 Core: 30.40 m; Schandelah Core: 50 and 51 m). In unit 3 of both cores calcareous nannofossils
225 display minor/moderate to moderate/major etching (E1/2 to E2/3) and negligible to moderate overgrowth (O0
226 to O2) with a general moderate/poor to moderate preservation. Calcareous nannofossil preservation observed
227 in lithological units 1 and 2 of both cores varies between moderate to good with generally minor to moderate
228 etching (E1 to E2) and minor overgrowth (O1). Samples characterized by a moderate/poor preservation with
229 moderate etching (E2) and moderate overgrowth (O2) are restricted to the "Monotis Bank" of the L1 Core
230 (15.00 m) and to the lower part of unit 1 of the Schandelah Core (26.50 to 26.00 m). Samples from the
231 uppermost unit 1 of the Schandelah Core (13.5 to 5.5 m) show poor to moderate preservation with moderate
232 to major etching (E2 to E3) and minor overgrowth (O1).

233 6.2. Biostratigraphy

234 6.2.1. L1 Core

235 A total of seven calcareous nannofossil events have been detected (Fig. 3) allowing the identification of, from
236 bottom to top, the *Lotharingius hauffii* Zone (NJ5) and the *Carinolithus superbus* Zone (NJ6). The oldest
237 investigated sample (31 m) is assigned to the earliest Toarcian NJ5b Subzone based on the presence of
238 *Crepidolithus impontus*. The FO of *C. superbus crassus* (24.9 m) defines the NJ5/NJ6 zonal boundary. In the
239 same sample the FO of *D. constans* is recognized. In the NJ6 Zone several biohorizons are encountered: the
240 LOs of *C. granulatus* (24.7 m), *P. liasicus distinctus* (24.5 m), *B. finchii* (24.1 m) and *B. grande* (23.45 m).
241 The large morphotype of *B. finchii* last occurs in this biozone as well (24.3 m), just before the LO of the
242 standard one. The uppermost investigated sample (15 m) is still included in the early Toarcian NJ6 Zone due
243 to the absence of *Discorhabdus striatus*, that is the zonal marker of the base of the NJ7 Zone.
244 Among the calcareous nannofossil assemblages of the upper NJ5b Subzone only sporadic specimens
245 attributable to genera *Bussonius*, *Lotharingius*, *Crepidolithus* and *Schizosphaerella* have been detected. An
246 important drop in abundance for *Schizosphaerella* was recorded at the base of the unit 3 (24. 9 m). This might
247 correspond to the "*Schizosphaerella* crisis" (sensu Casellato and Erba 2015) affecting both *S. punctulata* and
248 "small" *S. punctulata* (Fig. 8). Calcareous nannofossil assemblages of the lower NJ6 Zone are dominated by
249 genera *Crepidolithus* (*Crepidolithus crassus* and *Crepidolithus impontus*) and *Lotharingius* (*Lotharinigius*
250 *hauffii*, *Lotharingius frodoi*, *Lotharingius barozii* and *Lotharingius sigillatus)*. A slight decrease in abundance
251 of genera *Biscutum*, *Bussonius*, *Calyculus*, *Carinolithus* and *Ortogonoides* was observed above the T-OAE. In
252 the L1 Core, genera *Biscutum*, *Bussonius*, *Calyculus*, *Carinolithus*, *Mitrolithus*, *Schizosphaerella* and
253 *Ortogonoides* are subordinate, and *Axopodorhabdus*, *Discorhabdus*, *Diductius*, *Parhabdolithus* and
254 *Tubirhabdus* occur sporadically.
255

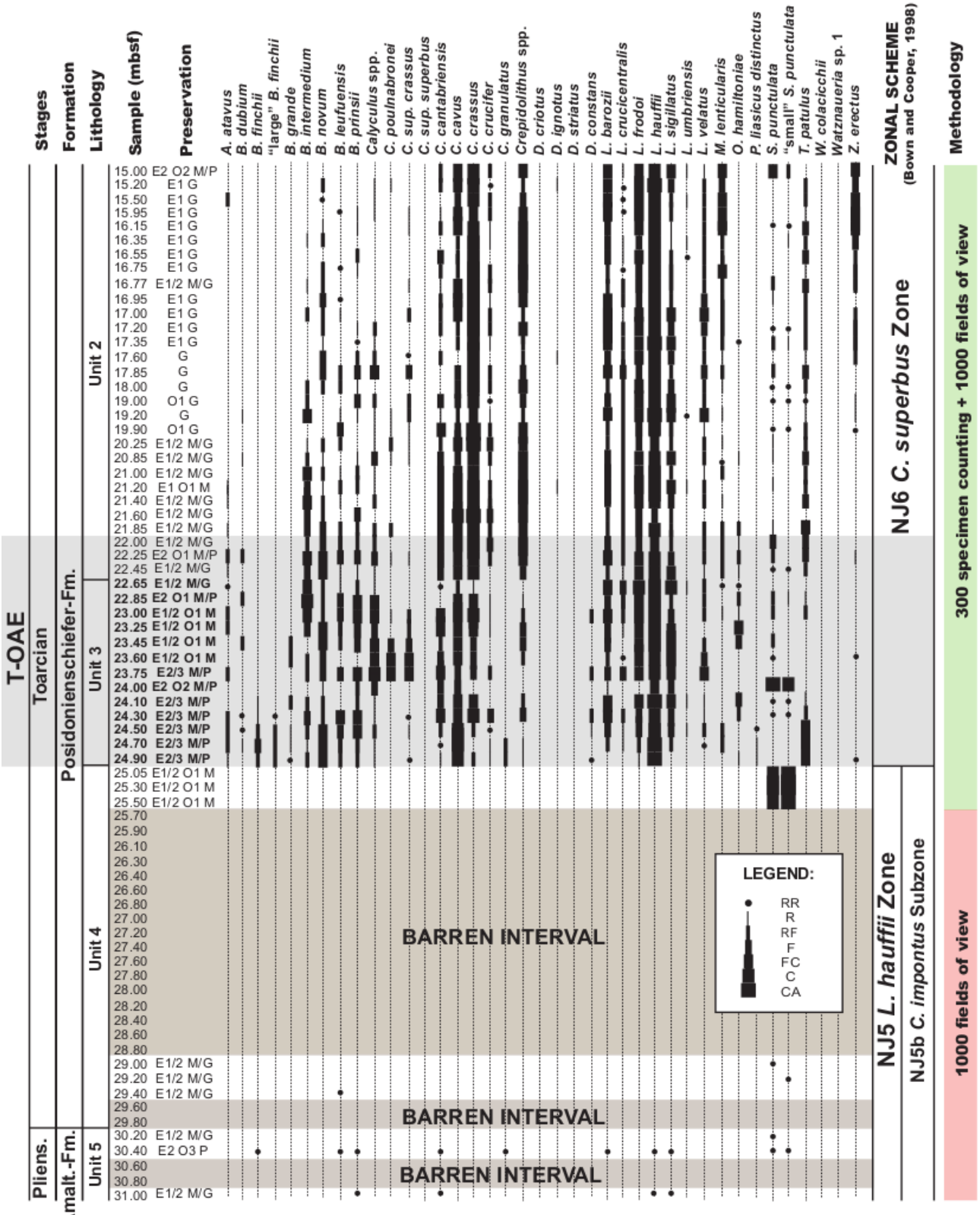

256 Fig. 5

257 6.2.2. Schandelah Core

258 A total of fifteen calcareous nannofossil events were used to define the *Lotharingius hauffii* Zone (NJ5), the

259 *Carinolithus superbus* Zone (NJ6) and the *Discorhabdus striatus* Zone (NJ7). The lowermost investigated

sample (52 m) is assigned to the earliest Toarcian NJ5 Zone, specifically to the NJ5b *Crepidolithus impontus* Subzone based on the presence of *C. impontus*. The FO of *C. superbus crassus* (43 m) defines the NJ5/NJ6 zonal boundary. In the same sample the FO of *D. constans* is recognized. In the lower part of the NJ6 Zone several biohorizons are detected: the LOs of *C. granulatus*, *P. liasicus distinctus*, *B. finchii* (41.5 m) and *B. grande* (40.5 m), as well as the last occurrence of the large morphotype of *B. finchii* (42.5 m). In the upper part of the NJ6 Zone an important drop in abundance of *L. hauffii* is here reported as the LO of the *L. hauffii* acme (31.5 m). The FO of *D. striatus* (28 m) defines the NJ6/NJ7 zonal boundary. At the same stratigraphic level, the FO of *Watznaueria* sp. 1 is recognized. Within the late Toarcian NJ7 Zone five events are found: the FO of *C. superbus superbus* (26 m), the FO of *W. colacicchii* (24.5 m), the LO of *Orthogonoides hamiltoniae* (21.5 m), the FO of *Discorhabdus criotus* (19 m). The uppermost investigated sample (5.5 m) is still included in the late Toarcian NJ7 Zone due to the absence of *Retecapsa incompta,* zonal marker of the NJ8 Zone.

Specimens attributable to genera *Bussonius*, *Lotharingius*, *Crepidolithus* and *Schizosphaerella* have been found sporadically in the upper part of Subzone NJ5b. The "*Schizosphaerella* crisis" (sensu Casellato Erba) was not recognized in the Schandelah Core since no significant drop in abundance of *Schizosphaerella* was observed (Fig. 8). The calcareous nannofossil assemblages characterizing the NJ6 Zone are dominated by *Crepidolithus* (*C. crassus*, *C. impontus*) and *Lotharingius* (*L. hauffii*, *L. frodoi*, *L. barozii*, *L. sigillatus*). A slight decrease in abundance of *Biscutum*, *Bussonius*, *Calyculus*, *Carinolithus* and *Ortogonoides* was encountered above the termination of the T-OAE. An increase in abundance of *Schizosphaerella* (22.0 m), the "*Schizoshaerella* recovery" (sensu Casellato and Erba, 2015), affecting both *S. punctulata* and "small" *S. punctulata* was recorded within the NJ7 biozone (Fig. 8). Genera *Crepidolithus* and *Lotharingius* dominate the calcareous nannofossil assemblages of the NJ7 Zone. The decrease in abundance of *L. hauffii* is balanced by an increase of larger *Lotharingius*, (*Lotharingius crucicentralis*, *Lotharingius velatus*). An increase of *Bussonius* and *Discorhabdus* is also recorded. As for the L1 Core, in the Schandelah Core genera *Biscutum*, *Bussonius*, *Calyculus*, *Carinolithus*, *Mitrolithus*, *Schizosphaerella* and *Orthogonoides* are subordinate whereas *Axopodorhabdus*, *Discorhabdus*, *Diductius*, *Parhabdolithus*, *Tubirhabdus* and *Watznaueria* are rare.

Fig. 6

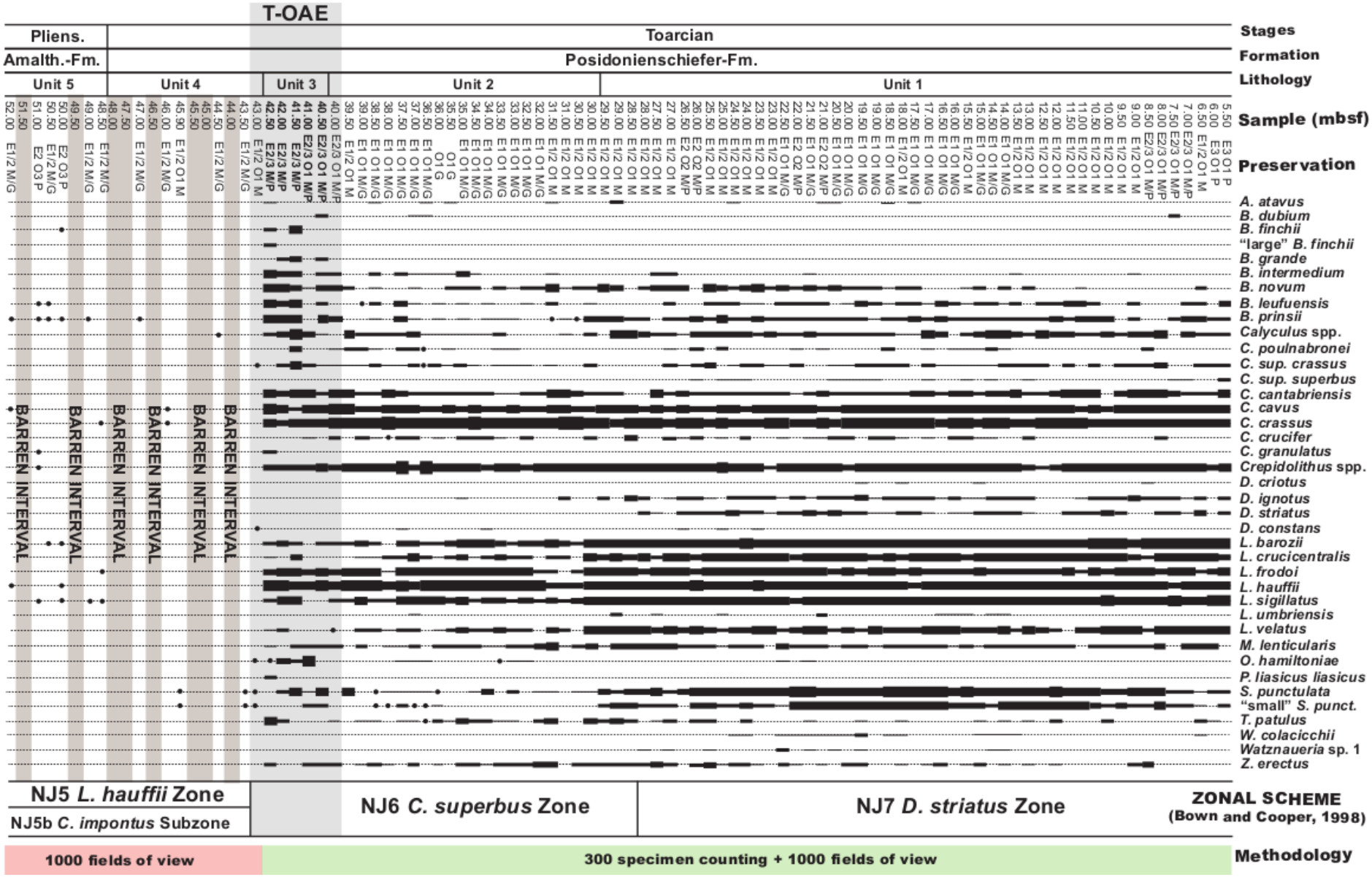
T-OAE
Pliens.
Toarcian
Stages
Amalth.-Fm.
Posidonienschiefer-Fm.
Formation
Unit 5
Unit 4
Unit 3
Unit 2
Unit 1
Lithology
Sample (mbsf)
Preservation
BARREN INTERVAL
A. atavus
B. dubium
B. finchii
"large" B. finchii
B. grande
B. intermedium
B. novum
B. leufuensis
B. prinsii
Calyculus spp.
C. poulnabronei
C. sup. crassus
C. sup. superbus
C. cantabriensis
C. cavus
C. crassus
C. crucifer
C. granulatus
Crepidolithus spp.
D. criotus
D. ignotus
D. striatus
D. constans
L. barozii
L. crucicentralis
L. frodoi
L. hauffii
L. sigillatus
L. umbriensis
L. velatus
M. lenticularis
O. hamiltoniae
P. liasicus liasicus
S. punctulata
"small" S. punct.
T. patulus
W. colacicchii
Watznaueria sp. 1
Z. erectus
NJ5 L. hauffii Zone
NJ5b C. impontus Subzone
NJ6 C. superbus Zone
NJ7 D. striatus Zone
ZONAL SCHEME
(Bown and Cooper, 1998)
1000 fields of view
300 specimen counting + 1000 fields of view
Methodology

6.3. Geochemistry

Bulk rock carbonate of the L1 Core varies from 0 % (samples in units 5 and 4 except for the concretionary layers) to 90 % at 15 m (*Monotis* Bank). As far as the Schandelah Core is concerned, it varies from 0 % (samples in units 5 and 4 except for the concretionary layers) to 81% at 31.5 m (*Monotis* Bank). For the L1 Core $\delta^{13}C_{org}$ values range from -25.18 ± 0.08 ‰ at 27.4 m to -33.13 ± 0.08 ‰ at 23.75 m. The most negative values are restricted to the carbon isotope excursion (CIE) detected in unit 3 (samples from 24.9 m to 22.65 m). In the Schandelah Core, $\delta^{13}C_{org}$ values range from -25.71 ± 0.08 ‰ at 49 m to -32.78 ± 0.08 ‰ at 41.5 m. As for the former core, unit 3 displays the most negative values (samples from 42.5 m to 40.5 m).

7. Discussion

7.1. Comparison of the L1 and Schandelah cores.

Calcareous nannofossil preservation, biostratigraphy, abundance, calcium carbonate and organic carbon isotope data display very consistent results between the two investigated cores, although a general slightly higher degree of overgrowth was noted in the Schandelah Core. This slightly stronger diagenetic overprint may be attributed to a more evolved sediment maturity in Schandelah. The FOs of *C. superbus crassus*, *D. constans* and the LOs of *P. liasicus distinctus, C. granulatus*, "large" *B. finchii, B. finchii* and *B. grande* appear consistent in the two cores. Little differences regarding the event positions depend on the different sampling densities adopted (higher in the L1 Core). Consequently, some events were detected within the same sample in the Schandelah Core (i.e., LOs of *P. liasicus distinctus, C. granulatus*, "large" *B. finchii* in sample 42.5 m) (Fig. 4). The FOs of *C. superbus crassus* and *D. constans* were recognized in the uppermost unit 4 in the Schandelah Core while they were found in the lowermost unit 3 in the L1 Core due to the presence of a hiatus (Fig. 3). Calcareous nannofossil variations in abundance are also very consistent.

The only remarkable difference observed regards the genus *Schizosphaerella*. A meaningful drop in abundance at the base of the shale was noted exclusively in the L1 Core (Fig. 8). No variation in abundance was observed in the Schandelah Core making the recognition of the "*Schizosphaerella* crisis" impossible. This fact is imputed by the sporadic presence of nannofossils, including *Schizosphaerella*, in units 5 and 4. The potential recognition of the "*Schizosphaerella* crisis" exclusively in the L1 Core is based on three samples below the Posidonienschiefer (i.e., 25.5 m, 25.3 m, 25.05 m) that contain abundant *Schizosphaerella* specimens. The "*Schizosphaerella* crisis", marked by an average decrease of both abundance and size, is an event documented

by several authors at lower latitudes (e.g., Mattioli and Pittet 2002, Suan et al. 2008, 2010, Casellato and Erba 2015) and at higher latitudes (e.g., Mailliot et al. 2009, Clémence et al. 2015, Peti and Thibault 2017) at the base of the T-OAE. In the NGB, the "*Schizosphaerella* crisis*"* is hampered by the sporadic presence of nannofossils in the lowermost part of the Posidonienschiefer-Fm. (Unit 4).

7.2. Comparison with van de Schootbrugge et al. (2019)

Calcareous nannofossil biostratigraphy carried out by van de Schootbrugge et al. (2019) in the Schandelah Core displays analogies and differences with our investigation (Fig. 3). For the corresponding stratigraphic interval two events were reported in their study (i.e., FOs of *C. superbus* and *D. striatus*) (van de Schootbrugge et al. 2019: Fig. 3). The FO of *D. striatus* detected at 25 m displays a quite good analogy with our datum (28 m) whereas the FO of *C. superbus* (*C. superbus crassus* in this work) is less consistent being detected 9 meters above our result (34 m versus 43 m). It is important to state, however, that the sampling rate adopted by van de Schootbrugge et al. (2019) is different from that used in this work. The authors, indeed, chose an interval varying between 1 to 3 meters which is perfectly suitable for their purpose, since their investigation spans 338 m of sediments from the Rhaethian to the Toarcian, but definitively lower once compared to that adopted in the present analysis (one sample/50 cm). Considering the samples prepared with the same method and the number of fields of views examined for each smear slides analogous to that here adopted we conclude that the reason of such a discrepancy is imputed to sample density resolution. For the same motivation, indeed, the taxa last occurring within the lower part of the T-OAE and being present continuously in a relatively short interval, from 43 m to 40.5 m, (i.e., LOs of *C. granulatus*, *P. liasicus distinctus*, *B. finchii*, *B. grande*), were not considered in the analysis conducted by van de Schootbrugge et al. (2019). The remaining events (i.e., FOs of *D. constans*, *Watznaueria* sp.1, *W. colacicchi*, *D. criotus* and LOs of *O. hamiltoniae)* were not reported in their analyses probably also for the scatter occurrence of the relative taxa which may have prevented the assessment of their FOs/LOs. Additionally, van de Schootbrugge et al. (2019) found the "*Schizosphaerella* crisis" and detected it slightly above the Pliensbachian/Toarcian boundary but without specifying the exact position. Consistently to the L1 Core in the present work, the authors might have considered a stratigraphic level (potentially a concretion) richer in schizosphaerellids followed by a drop in abundance of the taxon. However, being the Aamalthenton-Fm and the lower part of the Posidonienschiefer-Fm (units 5 and 4) mainly

barren of nannofossils, it is hard to assess whether we are dealing with the "*Schizosphaerella* crisis" or a temporary drop in abundance of schizosphaerellids.

7.3. Comparison with the standard biozonation scheme.

Calcareous nannofossil events recognized in the L1 and Schandelah cores (Fig. 7) are compared to the biohorizons used in the Boreal zonation of Bown and Cooper (1998). For the latest Pliensbachian to late Toarcian time interval (*Pleuroceras spinatum* to *Haugia variabilis* ammonite zones) the authors reported 9 calcareous nannofossil events (FO of *C. impontus*, FO of *L. sigillatus*, LO of *C. primulus*, FO of *C. superbus*, LO of *B. finchii*, LO of *O. hamiltoniae*, FO of *D. striatus*, FO of *D. criotus*, LO of *L. hauffii* acme) and defined three zones (NJ5, NJ6 and NJ7).

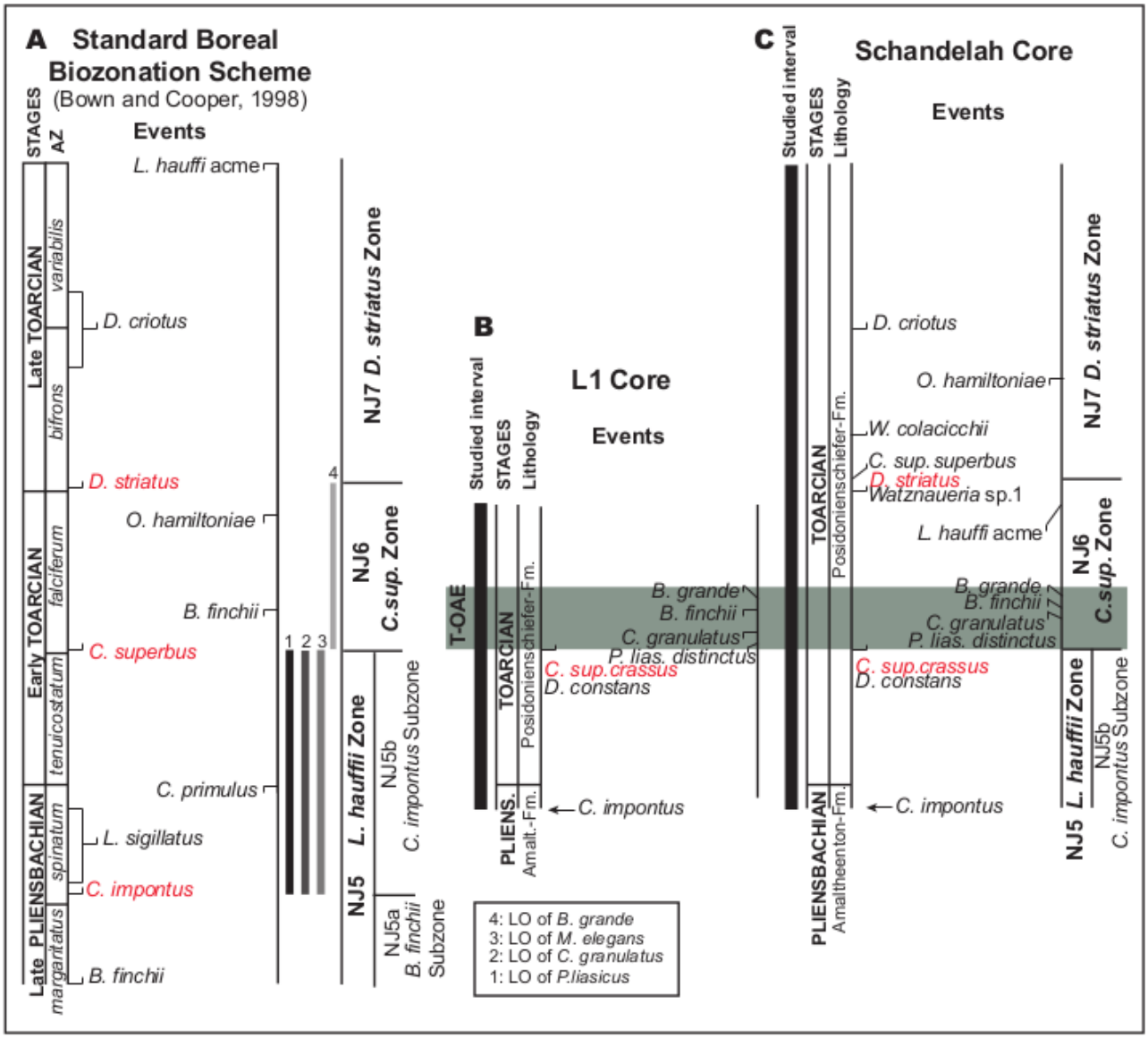

Fig. 7

The presence of *C. impontus* and *L. sigillatus* was documented from the base of both cores. Specimens of *C. primulus* were not found, probably for the rareness of nannofossils in units 5 and 4, preventing the recognition of its LO. The other biohorizons of Bown and Cooper (1998) have been recognized although with minor differences in their succession relative to the standard biozonation scheme. The FOs of *C. superbus crassus*, *D. striatus*, *D. criotus* and the LO of *B. finchii* are consistent with the datums reported by Bown and Cooper (1998). The LO of *O. hamiltoniae* was detected slightly before the FO of *D. criotus* in the studied material, whereas Bown and Copper (1998) reported this event slightly before the FO of *D. striatus*. This difference is most probably imputed by the rareness of *O. hamiltoniae* during its final range that weakens its reliability as marker species. This taxon seems to have a strong affinity with organic-rich sediments in the studied cores (Figs. 5, 6) being a fundamental constituent of calcareous nannofossil assemblages during the T-OAE (unit 3) in both the L1 and the Schandelah cores. Following the organic carbon isotope anomaly nannofossil abundance decreases drastically and becomes sporadic. In order to recognize the *L. hauffii* acme reported by Bown and Cooper (1998), we compiled the abundances of this taxon across the studied cores (Fig. 8). A remarkable drop in abundance was observed at 31.5 m (*L. hauffii* acme): this latter, however, does not correlate to that reported in the zonal scheme, probably because fluctuations in abundance of this taxon depends on local paleoenvironmental conditions (Ferreira et al. 2017).

In addition to nine well defined biohorizons, Bown and Cooper (1998: Fig. 4.1) discussed four additional, nannofossil bioevents in the Toarcian interval. Those are the LOs of *P. liasicus distinctus, M. elegans* and *C. granulatus* within the NJ5b Subzone and the LO of *B. grande* within the NJ6 Zone without specifying the precise stratigraphic position of these events. Except for the LO of *M. elegans*, which was not detected in this study probably for the scarcity of nannofossils in units 5 and 4, the other events have been recognized in both cores. Unlike Bown and Cooper (1998), the LOs of *P. liasicus distinctus* and *C. granulatus* were both observed in the lowermost NJ6 Zone in our study, thus displaying minor differences with the zonal scheme. The LO of *B. grande,* being recognized in the NJ6 in our investigation, shows consistent results with the zonal scheme. Specifically, our investigation reveals that all these LOs (*C. granulatus, P. liasicus distinctus, B. finchii, B. grande*) were recognized within the $\delta^{13}C_{org}$ isotope excursion of the T-OAE. Other calcareous nannofossil events (i.e., FO of *D. constans*, FO of *Watznaueria* sp.1, FO of *W. colacicchii*) observed here, were not reported in the standard zonal scheme.

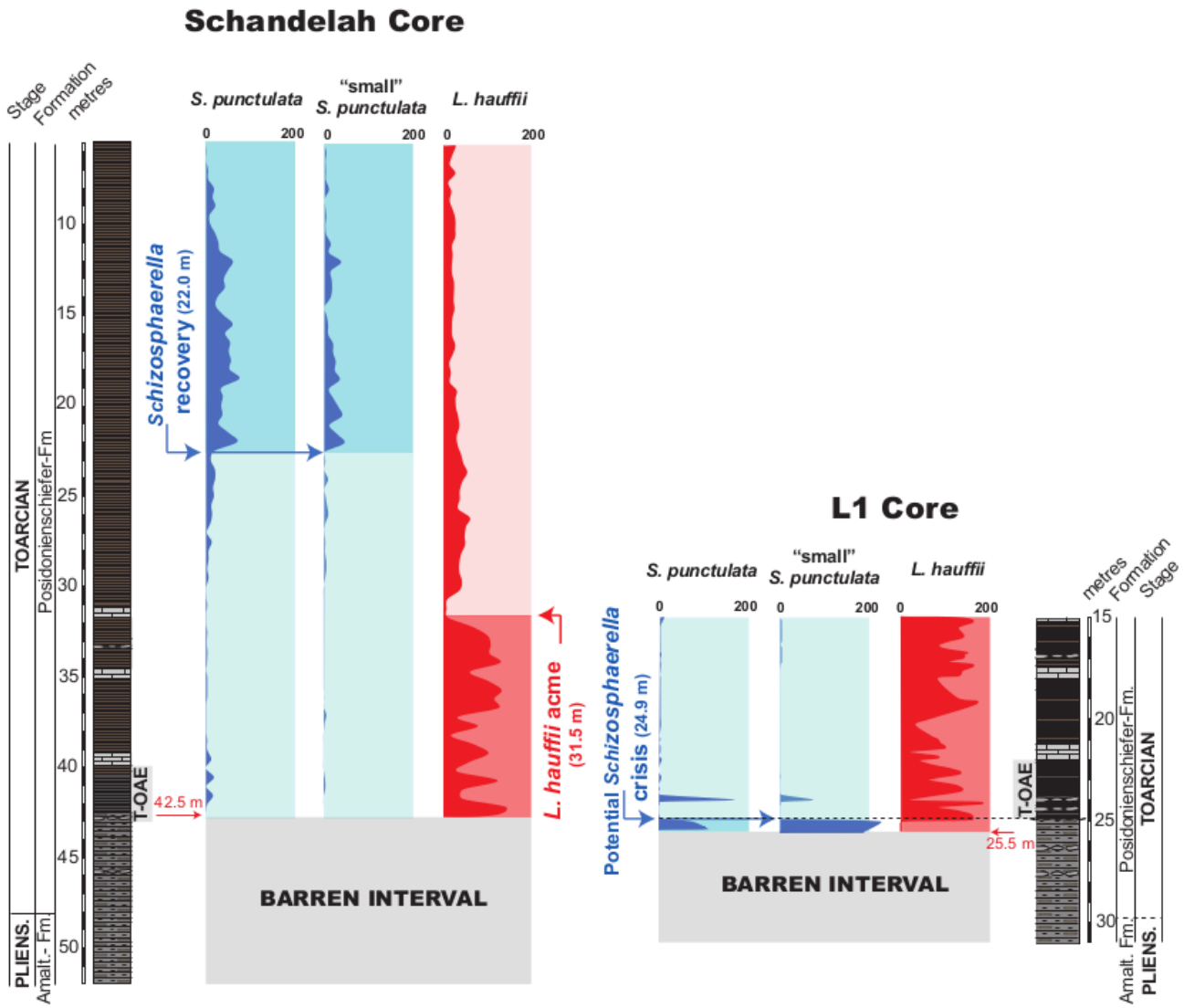

379 Fig. 8

380 7.4. A new biostratigraphic database for a more refined subdivision of the T-OAE at higher latitudes?

381 The late Pliensbachian - early Toarcian interval was a crucial time for calcareous nannofossil evolution as a
382 major speciation took place. Some of the most common Jurassic and Cretaceous genera appeared and evolved
383 rapidly (Bown 1987, Mattioli and Erba 1999, Bown et al. 2004, Erba 2004, 2006). As a result, the high number
384 of biostratigraphic events characterizing the late Pliensbachian - early Toarcian period offers the opportunity
385 to biostratigraphically constrain the T-OAE. The dataset for the Boreal Realm is, however, poor and less
386 resolutive compared to that of the Tethys. In particular, very few studies display the geochemical
387 characterization of the T-OAE together with a high resolutive calcareous nannofossil biostratigraphy provided
388 with range charts (e.g., Menini et al. 2019). As a result, potential biostratigraphic constrains and related
389 calibration with isotope anomalies remain poorly investigated in the Boreal Realm.

In order to evaluate diachroneity and reproducibility of individual calcareous nannofossil events prior, during and after the T-OAE, Casellato and Erba (2015: Figs. 6, 7) compared biohorizons against ammonite biozones and the $\delta^{13}C$ excursion. The relevant interval was sandwiched by the FOs of *Calyculus* and *D. striatus* of the zonation of Mattioli and Erba (1999). In the present work several calcareous nannofossil events were detected prior and during the T-OAE (FOs of *C. superbus crassus*, *D. constans;* LOs of *P. liasicus distinctus*, *C. granulatus*, *B. finchii*, *B. grande*). Apart from the former, the other biohorizons were not included in the analyses conducted by Casellato and Erba (2015). We compare the six biohorizons observed in the two studied cores against the $\delta^{13}C$ curve (Fig. 9) as documented for the other sections at higher latitudes (Germany, France, England, northern Spain) and those at lower latitudes (Italy, southern and eastern Spain, Hungary, Greece, Portugal) (see Tab. 1 for references). Although northern Spain and Portugal were located at higher and lower latitudes respectively, in this analysis they are separated from sections belonging to the Boreal and Tethyan Realms since calcareous nannofossil display peculiar assemblages in these regions. In fact, two specific zonal schemes exist for northern Spain and Portugal: the one of Fraguas et al. (2015) integrated in Fraguas et al. (2018) and that of Ferreira et al. (2019) based upon sections belonging to the Cantabrian Range and Lusitanian Basin, respectively.

As the $\delta^{13}C$ curves available for most of the considered sections have a low resolution, a generalized curve (Hesselbo et al. 2007: Fig. 1) is used. Based on the $\delta^{13}C$ curve of the two cores studied here, in Fig. 9 we distinguish a total of six sub-intervals from bottom to top: lowermost Toarcian recovery following the negative excursion at the Pliensbachian/Toarcian boundary (sub-interval a); pre T-OAE anomaly (sub-interval b); rapid decrease (sub-interval c); minimum (sub-interval d); recovery (sub-interval e) and post T-OAE anomaly (sub-interval f).

The aim is to evaluate whether these calcareous nannofossil biohorizons may be considered as additional events constraining the T-OAE on a global or regional scale or whether they are restricted to the North German Basin.

The FO of *C. superbus crassus*, an event already discussed by Casellato and Erba (2015), was encountered within sub-interval b in both cores. However, only the datum from Schandelah is reliable for the absence of the hiatus. Our result is consistent with findings from other sections. It needs to be stated, however, that this event is also reported to occur within sub-interval c from various sections (see Fig. 9 for details). This minor

discrepancy is probably imputed to the different sample density adopted in each study. The optimal reliability and reproducibility displayed by the FO of *C. superbus crassus* suggests and further reinforce that this bio-event is an excellent tool to correlate the onset of the T-OAE on a supraregional scale as previously pointed out by Mattioli et al. (2004a, 2013) and Casellato and Erba (2015).

The remaining events were detected only in few sections, thus showing a weaker reproducibility.

The FO of *D. constans* was found in sub-interval b in both cores. As for *C. superbus crassus*, only the datum from Schandelah is reliable. Our results correspond to observations in central Portugal (Peniche section). In northern Italy (Colle di Sogno section) this event fell into sub-interval c, whereas it occurred in northern Portugal (Rabaçal section) at a much younger level in the NJT7b (Middle Toarcian). In central France (Anse St. Nicolas section) the FO of *D. constans* was detected in the sub-interval a (Fig. 9). The datum proposed for northern Portugal is much younger compared to that from central Portugal probably because for the spotty occurence of this taxon. The datum recognized in central France is slightly older than that recorded for the L1 and Schandelah cores, suggesting an older age of this event in the Boreal Realm. The FO *D. constans* documented at Anse St. Nicolas is probably more reliable than that recorded in the L1 and Schandelah cores, because the lower parts of the investigated cores are essentially barren of nannofossils, probably preventing the recognition of the real FO of this taxon.

Although a potential utility as biostratigraphic marker for the onset of the T-OAE is not excluded, further investigations are recommended to verify the reliability and reproducibility of the FO of *D. constans*.

The LO of *P. liasicus distinctus* was detected within sub-interval b in both cores. This event was detected within the sub-interval c in central France (Sancerre-Couy section). The presence of this taxon was documented in northern Italy (Colle di Sogno section) after the T-OAE (Fig. 9).

The LO of *B. finchii* was observed in the lowermost sub-interval d in both cores. An analogous result was documented for central France (Sancerre-Couy section). This event fell into the sub-interval f in Hungary (Reka section). The presence of this taxon was documented in northern Italy and Greece (Colle di Sogno and Toka sections) after the T-OAE (Fig. 9).

The LO of *B. grande* was found in sub-interval d in the L1 Core and in sub-interval e in the Schandelah Core. The datum reported for the former succession is analogous to that proposed for central France (Sancerre-Couy

445 section). The presence of this taxon was documented in northern Italy (Colle di Sogno section) after the T-
446 OAE (Fig. 9).
447 The levels of the LOs of *P. liasicus distinctus, B. finchii, B. grande* detected in the L1 and Schandelah cores
448 are consistent with those of central France, namely, within the C isotope anomaly of the T-OAE. In the
449 Sancerre-Couy section, however, the LO of *P. liasicus distinctus* was detected at a younger stratigraphic level
450 compared to the LO of *B. finchii*. Although this minor discrepancy, we confirm that these events are reliable
451 in these regions of the Boreal Realm (northern Germany and central France) in accordance with the zonal
452 scheme of Bown and Cooper (1998). However, it needs to be stated that in other Lower Toarcian sections from
453 the Boreal Realm these events were not reported (i.e., Dotternhausen, Brown Moor, Andra, Tornadous, Anse
454 St. Nicolas). This is due to the fact that some of these biostratigraphic studies focused on a slightly lower
455 stratigraphic interval where these taxa still occur (Anse St. Nicolas) whereas in others the authors reported
456 exclusively the main events (Dotternhausen, Brown Moor, Andra, Tournadous) without providing range
457 charts, thus, preventing the possibility of discussing the distribution of these taxa.
458 Bown and Cooper (1998) reported these events in the biozonation scheme without specifying any correlation
459 with the T-OAE. Based on carbon isotope data evidencing the T-OAE anomaly, we confirm their utility as
460 biostratigraphic constrains of the T-OAE at least in northern Germany and, potentially, also in central France.
461 Further investigations are however required to confirm their reliability as biostratigraphic constrains of the T-
462 OAE in other regions of the Boreal Realm (e.g., southern Germany, England).
463 At lower latitudes these events are younger as documented in northern Italy and Greece. In fact, the zonal
464 scheme for the Tethyan Realm of Mattioli and Erba (1999) placed these events in the Lower (LO of *P. liasicus*
465 *distinctus*) and Upper Aalenian (LOs of *B. grande* and *B. finchii*). These events are younger also in Portugal
466 as pointed out by the recently published biozonation scheme of Ferreira et al. (2019) where these taxa are
467 present up to lowermost Bajocian. The biozonation for northern Spain of Fraguas et al. (2015) attests the
468 presence of these taxa up to the top of the investigated interval (Lower Toarcian *Harpoceras Serpentinum* AZ)
469 which is stratigraphically slightly lower than the level in which they are detected in the investigated cores.
470 Thus, their utility as biostratigraphic constrains of the T-OAE in northern Spain is not excluded.
471 The LO of *C. granulatus* was recognized in sub-interval c in both cores. The presence of this taxon was
472 documented in northern Italy (Colle di Sogno section) after the T-OAE (Fig. 9). This event was recognized

exclusively in the investigated German cores. It is younger in the Tethys (earliest Bajocian) as reported in northern Italy as well as in the zonal scheme of Mattioli and Erba (1999). This event is younger also in Portugal as certified by Ferreira et al. (2019) where this taxon is present up to lowermost Bajocian.

Although this event is not reported in northern Spain by Fraguas et al. (2015), based on range charts presented it is possible to discern a potential last occurrence at a stratigraphic level consistent with that identified in the L1 and Schandelah cores, which should be, however, further confirmed in other sections.

The LO of *Mitrolithus jansae*, an event approximating the termination of the T-OAE (Casellato and Erba, 2015) in the Tethys and Portugal was not recognized in the two cores. Specimens of this taxon were not found in the studied intervals, reinforcing the theory that *M. jansae* is a species better adapted to lower latitudes (Bucefalo Palliani et al. 2002, Mattioli et al. 2008, Reggiani et al. 2010, Fraguas et al. 2018).

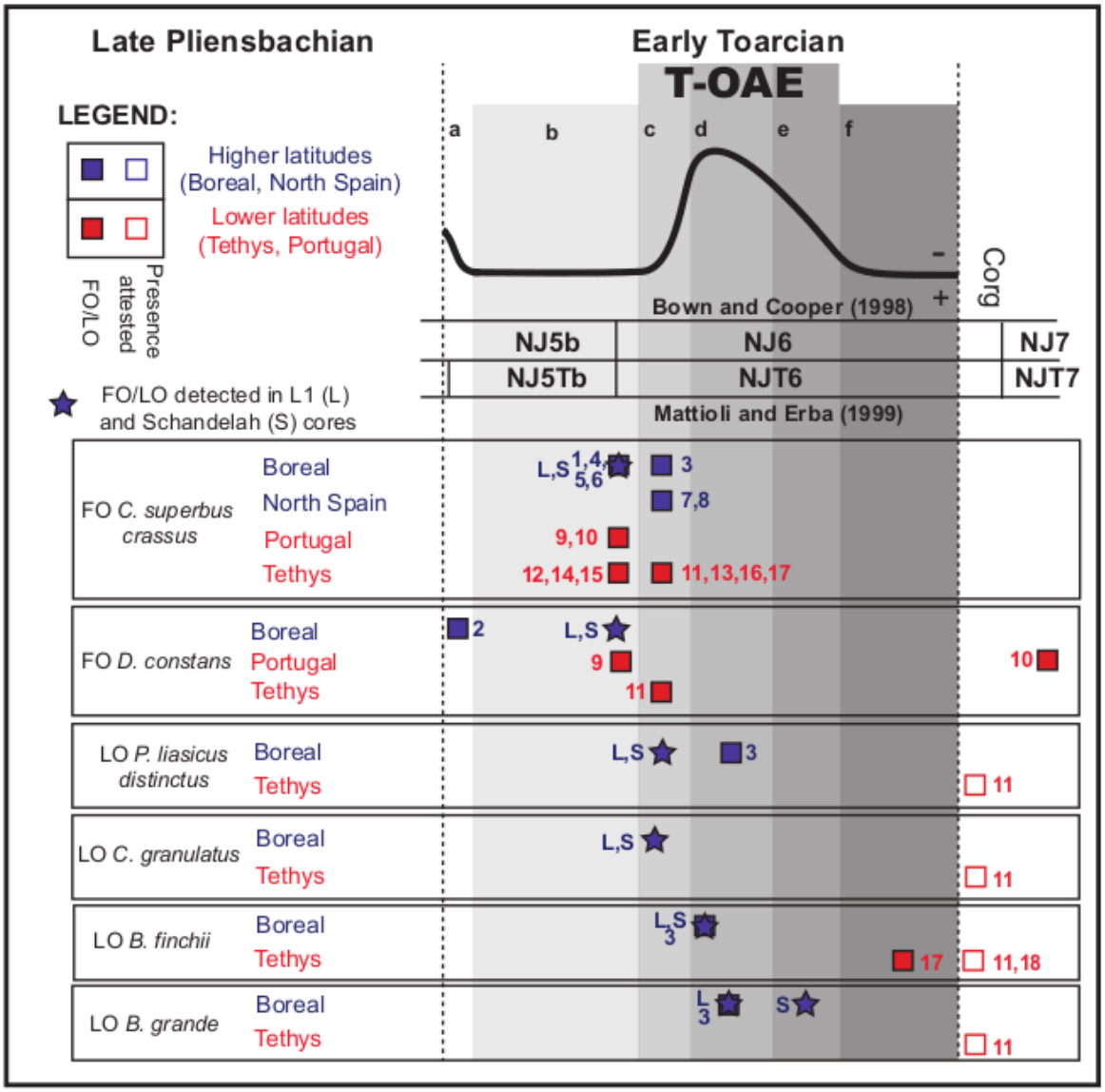

Fig. 9

Domain	Realm/Country	Country	Section	Reference
Higher latitudes	Boreal	North Germany	L1 Core (L)	This work
			Schandelah Core (S)	van de Schootbrugge et al. (2019), This work
		South Germany	Dotternhausen (1)	Mattioli et al. (2008)
		Central France	Anse St. Nicolas (2)	Menini et al. (2019)
			Sancerre-Couy (3)	Peti et al. (2017), Boulila et al. (2014)
			Tournadous (4)	Mailliot et al. (2009)
			Andra (5)	Mattioli et al. (2008)
		United Kingdom	Brown Moor (6)	Mattioli and Pittet (2004)
	North Spain	North Spain	West Rodiles (7)	Fraguas et al. (2012)
			Castillo de Pedroso (8)	Tremolada et al. (2005)
Lower latitudes	Portugal	Central Portugal	Peniche (9)	Mattioli et al. (2013), da Rocha et al. (2016)
		North Portugal	Rabaçal (10)	Ferreira et al. (2015, 2019)
	Tethys	North Italy	Colle di Sogno (11)	Erba (2004), Casellato and Erba (2015)
		Central Italy	Valdorbia (12)	Mattioli et al. (2013)
			Pozzale (13)	Mattioli and Pittet (2004)
			Somma (14)	Mattioli and Pittet (2002)
		South East Spain	La Almunia (15)	Menini et al. (2019)
			La Cerradura (16)	Sandoval et al. (2012), Reolid et al. (2014)
		Hungary	Reka (17)	Müller et al. (2017)
		Greece	Toka (18)	Kafousia et al. (2014)

Tab. 1

8. Conclusions

Calcareous nannofossil biostratigraphy allowed the identification of six (L1 Core) and fourteen calcareous nannofossil events (Schandelah Core) across the Amaltheenton-Fm. and Posidonienschiefer-Fm. Following the standard nannofossil zonation the NJ5b and NJ6 biozones were identified for the L1 Core, the NJ5b, NJ6, NJ7 biozones for the Schandelah Core. The events detected in the studied cores are relatively consistent with those of the standard zonation scheme. In addition, further biohorizons have been recognized (FO of *D. constans*, FO of *Watznaueria* sp.1, FO of *W. colacicchii*).

The T-OAE, identified on the basis of the $\delta^{13}C$ anomaly within the Posidonienschiefer-Fm., is defined by six calcareous nannofossil events. The FOs of *C. superbus crassus* and *D. constans* correspond to the onset of the isotope excursion. The LOs of *P. liasicus distinctus*, *C. granulatus*, *B. finchii* and *B. grande* were detected within the isotopic excursion. Calibration against the $\delta^{13}C$ anomaly reveals that the sequence of nannofossil biohorizons does not always correlate with those of other areas. The FO of *C. superbus crassus* displays a

supraregional reproducibility whereas the FO of *D. constans* is less reproducible and requires further investigations. The LOs of *C. granulatus, P. liasicus distinctus, B. finchii* and *B. grande* are restricted to the Boreal Realm in accordance with the Boreal zonal scheme. Our investigation reveals that these latter events are recognized within the $\delta^{13}C$ anomaly and can be used to further constrain the T-OAE in northern Germany and, potentially, in central France.

9. Acknowledgements

We are extremely grateful to various people without whom this project would have been impossible to realize. First of all, people working in the Wintershall-DEA oil company and in the core repository of the German Federal Institute of Geosciences and Natural Resources in Berlin Spandau who gave access to the cores. Their help and support are appreciated. The authors wish to thank M. Hillebrand for his contribution in collecting and preparing samples for geochemical investigations. A special thanks is going to L. Wulff, T. Püttmann and K. Stevens for their practical advice, help and availability. V.M. Giraldo Gómez is also thanked for his precious assistance. The quality of the manuscript was improved by the constructive comments of two anonymous reviewers for which we are grateful. This paper is one of the results of Stefano Visentin PhD co-funded by a DAAD short term grant and the Università degli Studi di Milano.

10. Appendix 1

Calcareous nannofossil taxa, reported in this study, are alphabetically ordered per genus, species and subspecies. Authors, date of the original description and, when necessary, emendations are provided.

Axopodorhabdus atavus (Grün et al. 1974) Bown (1987)

Biscutum dubium (Noël 1965) Grün *in* Grün et al. (1974)

B. finchii (Crux 1984) Bown (1987)

B. grande Bown (1987)

B. intermedium Bown (1987)

B. novum (Goy 1979) Bown (1987)

Bussonius leufuensis Bown and Kielbowicz (1987)

B. prinsii (Noël 1973) Goy (1979)

Calyculus Noël (1973)

Carinolithus cantaluppii (Cobianchi 1990)

525 *C. poulnabronei* Mattioli (1996)

526 *C. superbus* (Deflandre 1954) Prins *in* Grün et al. (1974)

527 *C. superbus crassus* Visentin and Erba *in* Visentin et al. (2021)

528 *C. superbus superbus* (Deflandre 1954) Prins *in* Grün et al. (1974)

529 *Crepidolithus cantabriensis* Fraguas (2014)

530 *C. crassus* (Deflandre *in* Deflandre and Fert 1954) Noël (1965)

531 *C. crucifer* (Prins 1969) ex Rood et al. (1973)

532 *C. granulatus* Bown (1987)

533 *C. impontus* Grün et al. (1974)

534 *Crucirhabdus primulus* (Prins 1969) ex Rood et al. (1973) Bown (1987)

535 *Diductius constans* Goy (1979)

536 *Discorhabdus criotus* Bown (1987)

537 *D. ignotus* (Gorka, 1957) Perch-Nielsen (1968)

538 *D. striatus* Moshkovitz and Ehrlich (1976)

539 *Lotharingius barozii* Noël (1973)

540 *L. crucicentralis* (Medd 1971) Grün and Zweili (1980)

541 *L. frodoi* Mattioli (1996)

542 *L. hauffii* Grün and Zweili *in* Grün et al. (1974)

543 *L. sigillatus* (Stradner 1961) Prins in Grün et al. (1974)

544 *L. umbriensis* Mattioli (1996)

545 *L. velatus* Bown and Cooper (1989)

546 *Mitrolithus elegans* Deflandre (1954)

547 *M. jansae* (Wiegand 1984) Bown *in* Young et al. (1986)

548 *M. lenticularis* Bown (1987)

549 *Ortogonoides hamiltoniae* Wiegand (1984)

550 *Parhabdolithus liasicus* Deflandre *in* Grassé (1952)

551 *Parhabdolithus liasicus distinctus* Bown (1987)

552 *Schizosphaerella punctulata* Deflandre and Dangeard (1938)

553 *Tubirhabdus patulus* Rood et al. (1973)

554 *Watznaueria colacicchii* Mattioli and Reale *in* Mattioli (1996)

555 *Watznaueria* sp.1 Cobianchi (1992)

556 **11. References**

557 Arp, G., Gropengießer, S., 2016. The Monotis-Dactylioceras Bed in the Posidonienschiefer Formation
558 (Toarcian Southern Germany): condensed section, tempestite, or tsunami generated deposit?
559 Paläontologische Zeitschrift 90, 2, 271-286.

560 Bassoullet, J.P., Elmi, S., Poisson, A., Cecca, F., Bellion, Y., Guiraud, R., Baudin, F., 1993. Mid Toarcian. In:
561 Dercourt J., Ricou L.E., Vrielynck B., (Eds.), Atlas Tethys Paleoenvironmental Maps. BEICIP –
562 FRANLAB, Rueil-Malmaison, France, p. 63-84.

563 Baldanza, A., Bucefalo Palliani, R., Mattioli, E., 1996. 3.5.4. Phytoplankton im Toarcium und Aalenium der
564 Forschungsbohrung KB Wittnau In*:* Ohmert, W., Allia, V., Arias, C., Baldanza, A., Bergen, J.A.,
565 Bucefalo Palliani, R., Canales, M.L., de Kaenel, E., Garcia Joral, F., Goy, A., Herrero, C., Höhndorf,
566 A., Martinez, G., Mattioli, E., Perilli, N., Riegraf, W., Rolf, Ch., Ureta, S., Wetzel, A., Wonik, T.
567 (Eds): Die Grenzziehung Unter/Mitteljura (Toarcium /Aalenium) bei Wittnau und Fuentelsaz. Bei-
568 spiele interdisziplinärer geowissenschaftlicher Zusammenarbeit. Geologisches Landesamt Baden-
569 Württemberg, Freiburg i., Informationem 8, p. 29-33.

570 Boulila, S., Galbrun, B., Huret, E., Hinnov, L.A., Rouget, I., Gardin, S., Bartolini, A., 2014. Astronomical
571 calibration of the Toarcian Stage: Implications for sequence stratigraphy and duration of the early
572 Toarcian OAE. Earth and Planetary Sciences Letters 386, 98-111.

573 Bown, P. R., 1987. Taxonomy, evolution, and biostratigraphy of Late Triassic-Early Jurassic calcareous
574 nannofossils. Palaeontolocial Association, Special papers in Palaeontology, 32, 118 p.

575 Bown, P.R., Cooper, M.K.E., Lord, A.R., 1988. A Calcareous Nannofossil Biozonation Scheme for the early
576 to mid-Mesozoic. Newsletters on Stratigraphy 20, 91-114.

577 Bown, P.R., Copper, M.K.E., 1998. Jurassic. In: Bown, P.R., (Ed.), Calcareous nannofossil biostratigraphy.
578 British Micropaleontological Society Published Series, Kluwer Academic Publishers, London, p. 34-
579 85.

580 Bown, P.R., Lees, J.A., Young, J.R., 2004. Calcareous nannoplankton evolution and diversity through time.
581 In: Thierstein, H.R., Young, J.R., (Eds.), Coccolithophores: from molecular processes to global
582 impact, Berlin., p. 481-508.
583 Bucefalo Palliani, R., Mattioli, E., Riding, J. B., 2002. The response of marine phytoplankton and sedimentary
584 organic matter to the early Toarcian (lower Jurassic) oceanic anoxic event in northern England. Marine
585 Micropalaentology 46, 223-245.
586 Casellato, C.E., Erba, E., 2015. Calcareous nannofossil biostratigraphy and paleoceanography of the Toarcian
587 Oceanic Anoxic event at Colle di Sogno (southern Alps, northern Italy). Rivista Italiana di
588 Paleontologia e Stratigrafia 121, 3, 297-327.
589 Clémence, M.E., Gardin, S., Bartolini, A., 2015. New insights in the pattern and timing of the Early Jurassic
590 calcareous nannofossil crisis. Palaeogeography, Palaeoclimatology, Palaeoecology 427, 100-108.
591 Cobianchi, M., 1990. Calcareous nannofossil biostratigraphy of the Domerian-Toarcian Boundary in the
592 Navezze Valley (Brescia). Atti Ticinensi di Scienze della Terra 33, 127-142.
593 Cobianchi, M., 1992. Sinemurian - Early Bajocian calcareous nannofossil biostratigraphy of the Lombardian
594 Basin (Southern calcareous Alps; Northen Italy). Atti Ticinensi di Scienze della Terra 35, 61-106.
595 Crux, J. A., 1984. Biostratigraphy of Early Jurassic calcareous nannofossils from southwest Germany. Neues
596 Jahrbuch für Geologie und Paläontologie Abhandlungen 169, 2, 160-186.
597 da Rocha, R.B., Mattioli E., Duarte, L., Pittet, B., Elmi, S., Mouterde, R., Cabral, M.C., Comas-Rengifo, M.,
598 Gomez, J., Goy, A., Hesselbo, S., Jenkyns, H., Littler, K., Mailliot, S., Veiga de Oliveira, L.C., Osete,
599 M.L., Perilli, N., Pinto, S., Ruget, C., Suan, G., 2016. Base of the Toarcian Stage of the Lower Jurassic
600 defined by the Global Boundary Stratotype Section and Point (GSSP) at the Peniche section (Portugal).
601 Episodes: Journal of International Geoscience 39, 3, 460-481.
602 Deflandre, G., Dangeard, L., 1938. Schizosphaerelle, un nouveau microfossile méconnu du jurassique moyen
603 et supérieur. Comptes Rendus des Seances de l'Academie des Sciences, 1115-1117.
604 Deflandre, G., Fert, C., 1954. Observations sur les coccolithophoridés actuels et fossiles en microscopie
605 ordinaire et électronique. Annales de Paléontologie 40, 115-176.

606 de Kaenel, E., Bergen, J.A., 1993. New early and Middle Jurassic coccolith taxa and biostratigraphy from the
607 eastern proto-Atlantic (Morocco, Portugal and DSDP Site 547 B). Eclogae Geologicae Helvetiae 86,
608 861-908.
609 de Kaenel, E., Bergen, J.A., 1996. 3.5.5. Kalkige Nannofossilien im Profil der Tongrube Wittnau. In*:* Ohmert,
610 W., Allia, V., Arias, C., Baldanza, A., Bergen, J.A., Bucefalo Palliani, R., Canales, M.L., de Kaenel,
611 E., Garcia Joral, F., Goy, A., Herrero, C., Höhndorf, A., Martinez, G., Mattioli, E., Perilli, N., Riegraf,
612 W., Rolf, Ch., Ureta, S., Wetzel, A., Wonik, T. (Eds): Die Grenzziehung Unter/Mitteljura (Toarcium
613 /Aalenium) bei Wittnau und Fuentelsaz. Beispiele interdisziplinärer geowissenschaftlicher
614 Zusammenarbeit. Geologisches Landesamt Baden-Württemberg, Freiburg i, Informationen 8, p. 33-
615 36.
616 Demaison, GJ., Moore G.T., 1980. Anoxic environments and oil source bed genesis. Organic Geochemistry
617 2, 1, 9-31.
618 Doornenbal, H., Stevenson, A., 2010. Petroleum geological atlas of the Southern Permian Basin area. EAGE,
619 342 p.
620 Erba, E., 2004. Calcareous nannofossils and Mesozoic oceanic anoxic events. Marine Micropaleontology 52,
621 85 -106.
622 Erba, E., 2006. The first 150 million years history of calcareous nannoplankton: Biosphere – Geosphere
623 interaction. Palaeogeography, Palaeoclimatology, Palaeoecology 232, 237-250.
624 Ferreira, J., Mattioli, E., Pittet, B., Cachao, M., Spangerberg, J.E., 2015. Palaeocological insights on Toarcian
625 and Lower Aalenian calcareous nannofossils from the Lusitanian Basin (Portugal). Palaeogeography,
626 Palaeoclimatology, Palaeoecology 436, 245-262.
627 Ferreira, J., Mattioli, E., van de Schootbrugge, B., 2017. Palaeoenvironmental vs. evolutionary control on size
628 variation of coccoliths across the Lower-Middle Jurassic. Palaeogeography, Palaeoclimatology,
629 Palaeoecology 465, 177-192.
630 Ferreira, J., Mattioli, E., Suchéras-Marx, B., Giraud, F., Duarte, L. V., Pittet, B., Suan G., Hassler A.,
631 Spangenberg, J. E., 2019. Western Tethys Early and Middle Jurassic calcareous nannofossil
632 biostratigraphy. Earth-Science Reviews 197, 1-19.

633 Fraguas, A., Comas-Rengifo, M.J., Gomez, J., Goy, A., 2012. The calcareous nannofossil crisis in Northen
634 Spain (Asturias province) linked to the Early Toarcian warming-driven mass estinction. Marine
635 Micropaleontology 94-95, 58-71.
636 Fraguas, A., Comas-Rengifo, M.J., Perilli, N., 2015. Calcareous nannofossil biostratigraphy of the Lower
637 Jurassic in the Cantabrian Range (Northen Spain). Newsletters on Stratigraphy 48, 179-199.
638 Fraguas, A., Comas-Rengifo, M. J., Goy, A., Gómez, J. J., 2018. Upper Sinemurian–Pliensbachian calcareous
639 nannofossil biostratigraphy of the E Rodiles section (Asturias, N Spain): a reference section for the
640 connection between the Boreal and Tethyan Realms. Newsletters on Stratigraphy 51, 227-244.
641 Frimmel, A., Oschmann, W., Schwark, L. 2004. Chemostratigraphy of the Posidonia Black Shale, SW
642 Germany. I. Influence of sea-level variation on organic facies evolution. Chemical Geology 206, 199
643 - 230.
644 Grün, W., Prins, P., Zweili, F., 1974. Coccolithophoriden aus dem Lias epsilon von Holzmaden
645 (Deutschland). Neues Jahrbuch für Geologie und Paläontologie. Abhandlungen 147, 294-328.
646 Hallam, A., 2001. A review of the broad pattern of Jurassic sea-level changes and their possible causes in the
647 light of current knowledge. Palaeogeography, Palaeoclimatology, Palaeoecology 167, 23-37.
648 Haq, B.U., Hardenbol J., Vail, P.R., 1988. Mesozoic and Cenozoic Chronostratigraphy and Cycles of Sea-
649 Level Change. In: Wilgus C. K. et al., (Eds.), Sea-Level Changes: An Integrated Approach. Special
650 Publications of Society for Economic Paleontology and Mineralogy 42, 198, 71–108.
651 Hauff, B., 1960. Das Holzmadenbuch., Hohenlohe, Öhringen, 80 p.
652 Hesselbo, S.H., Gröcke, D.R., Jenkins, H.C., Bjerrun, C.J., Farrimond, P., Morgans Bell, H.S., Green, O.R.
653 2000. Massive dissociation of gas hydrate during a Jurassic oceanic anoxic event. Nature 406, 392-
654 395.
655 Hesselbo, S. P., Jenkyns, H. C., Duarte, L. V., Oliveira, L. C. 2007. Carbon-isotope record of the Early Jurassic
656 (Toarcian) Oceanic Anoxic Event from fossil wood and marine carbonate (Lusitanian Basin,
657 Portugal). Earth and Planetary Science Letters 253, 3-4, 455-470.
658 Hoffmann, K. 1968. Die Stratigraphie und Paläogeographie der bituminösen Fazies des nordwestdeutschen
659 Oberlias (Toarcium). Beiheft Geologisches Jahrbuch 58, 443-498.

660 Jenkyns, H., 1988. The early Toarcian (Jurassic) anoxic event-stratigraphic, sedimentary, and geochemical
661 evidence. American Journal of Science 288, 2.
662 Jenkyns, H.C., Jones, C.E., Gröcke, D.R., Hesselbo, S.P., Parkinson, D.N., 2002. Chemostratigraphy of the
663 Jurassic System: applications, limitations and implications for palaeoceanography. Journal of the
664 Geological Society of London 159, 351–378.
665 Jenkyns, H. C., 2010. Geochemistry of oceanic anoxic events. Geochemistry, Geophysics, Geosystems 11, 3.
666 Kafousia, N., Karakitsios, V., Mattioli, E., Kenjo, S., Jenkyns, H.C., 2014. The Toarcian Oceanic Anoxic
667 Event in the Ionian Zone, Greece. Palaeogeography., Palaeoclimatology., Palaeoecology 393, 135-
668 145.
669 Kälin, O., 1980. *Schizosphaerella punctulata* Deflandre & Dangeard: wall ultrastructure and preservation in
670 deep-water carbonate sediments of the Tethyan Jurassic. Eclogae Geologicae Helvetiae 73, 3, 983-
671 1008.
672 Kälin, O., Bernoulli, D., 1984. *Schizosphaerella* Deflandre & Dangeard in Jurassic deeper-water carbonate
673 sediments, Mazagan Continental Margin (Hole 547B) and Mesozoic Tethys. Initial Reports DSDP 79,
674 411- 429.
675 Kemp, D.B., Coe, A.L., Cohen, A.S., Schwark, L., 2005. Astronomical pacing of methane release in the Early
676 Jurassic period. Nature 437, 396–399.
677 Kockel, F., Wehner, H., Gerling, P., 1994. Petroleum system of the Lower Saxony Basin, Germany: Chapter
678 34: Part VI. Case Studies – Eastern Hemisphere. AAPG Special volumes, p. 573-586.
679 Kockel, F., 2002. Rifting processes in NW-Germany and the German North Sea sector. Netherlands Journal
680 of Geosciences 81, 2, 149-158.
681 Kossow, D., Krawczyk, C. M., 2002. Structure and quantification of processes controlling the evolution of the
682 inverted NE-German Basin. Marine and Petroleum Geology 19, 5, 601-618.
683 Küspert, W., 1982. Environmental changes during oil-shale deposition as deduced from stable isotope ratios.
684 In: Einsele, G., Seilacher, A. (Eds.), Cyclic and Event Stratification. Springer, Berlin, p. 482–501.
685 Mailliot, S., Mattioli, E., Guex, J., Pittet, B., 2006. The Early Toarcian anoxia, a synchronous event in the
686 Western Tethys? An approach by quantitative biochronology (Unitary Associations), applied on
687 calcareous nannofossils. Palaeogeography. Palaeoclimatology, Palaeoecology 240, 562-586.

688 Mailliot, S., Mattioli, E., Bartolini, A., Baudin, F., Pittet, B., Guex, J., 2009. Late Pliensbachian–Early Toarcian
689 (Early Jurassic) environmental changes in an epicontinental basin of NW Europe (Causses area, central
690 France): A micropaleontological and geochemical approach. Palaeogeography. Palaeoclimatology,
691 Palaeoecology 273, 346-364.
692 Mattioli, E., Erba, E., 1999. Synthesis of calcareous nannofossil events in tethyan Lower and Middle Jurassic
693 successions. Rivista Italiana di Paleontologia e Stratigrafia 105, 3,343-376.
694 Mattioli E., Pittet B., 2002. Contribution of calcareous nannoplankton to carbonate deposition: a new approach
695 applied to the Lower Jurassic of Central Italy. Marine Micropaleontology 45, 175-190.
696 Mattioli, E., Pittet, B., 2004. Spatial and temporal distribution of calcareous nannofossil along a proximal-
697 distal transect in the Lowe Jurassic of the Umbria-Marche Basin (Central Italy). Palaeogeography.,
698 Palaeoclimatology., Palaeoecology 205, 295-316.
699 Mattioli, E., Pittet, B., Palliani, R., Röhl, H. J., Schmid-Röhl, A., Morettini, E., 2004a. Phytoplankton evidence
700 for the timing and correlation of palaeoceanographical changes during the early Toarcian oceanic
701 anoxic event (Early Jurassic). Journal of the Geological Society 161, 4, 685-693.
702 Mattioli, E., Pittet, B., Young, J.R., Bown, P.R., 2004b. Biometric analysis of Pliensbachian-Toarcian (Lower
703 Jurassic) coccoliths of the family Biscutaceae: intra and interspecific variability versus
704 palaeoenvironmental influence. Marine Micropaleontology 52, 5-27.
705 Mattioli, E., Pittet, B., Suan, G., Mailliot, S., 2008. Calcareous nannoplankton changes across the early
706 Toarcian oceanic anoxic event in the western Tethys. Paleoceanography 23, PA3208.
707 Mattioli, E., Pittet B., Petipierre, L., Maillot, S., 2009. Dramatic decrease of pelagic carbonate production by
708 nannoplankton across the Early Toarcian anoxic event (T-OAE). Global and Planetary Change 65, 134
709 - 145.
710 Mattioli, E., Plancq, J., Boussaha, M., Duarte, L.V., Pittet, B., 2013. Calcareous nannofossil biostratigraphy:
711 new data from the Lower Jurassic of the Lusitanian Basin. Comunicaçoes Geològicas 100, Especial I,
712 69-76.
713 McElwain, J.C., Wade-Murphy, J., Hesselbo, S.P., 2005. Changes in carbon dioxide during an oceanic anoxic
714 event linked to intrusion into Gondwana coals. Nature 435, 479–482.

715 Menini, A., Mattioli, E., Spangenberg, J. E., Pettit, B., Guillaume, S., 2019. New calcareous nannofossil and
716 carbon isotope data for the Pliensbachian/Toarcian boundary (Early Jurassic) in the western Tethys
717 and their paleoenvironmental implications. Newsletters on Stratigraphy 52, 2, 173-196.
718 Müller, G., Gastner, M., 1971. The "Karbonat-Bombe", a simple device for the determination of the carbonate
719 content in sediments, soils and other materials. Neues Jahrbuch fur Mineralogie, Monatshefte 10, 466
720 – 469.
721 Müller, T., Price, G.D, Bajnai, D., Nyerges, A., Kesjar, D., Raucsik, B., Varga, A., Judik, K., Fekete, J., May,
722 Z., Palfy, J., 2017. New multiproxy record of the Jenkyns Event (also known as the Toarcian Oceanic
723 Anoxic Event) from the Mecsek Mountains (Hungary): Differences, duration and drivers.
724 Sedimentology 64, 66-86.
725 Peti, L., Thibault, N., 2017. Abundance and size changes in the calcareous nannofossil *Schizosphaerella* -
726 Relation to sea-level, the carbonate factory and palaeoenvironmental change from the Sinemurian to
727 earliest Toarcian of the Paris Basin. Palaeogeography, Palaeoclimatology, Palaeoecology 485, 271-
728 282.
729 Peti, L., Thibault, N., Clémence, M.E., Korte, C., Dommergues, J.L., Bougealt, C., Pellenard, P., Jelby, M E.,
730 Ulmann, C.V., 2017. Sinemurian–Pliensbachian calcareous nannofossil biostratigraphy and organic
731 carbon isotope. Palaeogeography, Palaeoclimatology, Palaeoecology 468, 142-161.
732 Picotti, V., Cobianchi, M. 1996. Jurassic periplatform sequences of the Eastern Lombardian Basin (Southern
733 Alps): The deep-sea record of the tectonic evolution, growth and demise history of a carbonate
734 platform. Memorie di Scienze Geologiche 48, 171-219.
735 Reggiani, L., Mattioli, E., Pittet, B., Duarte, L.V., Veiga de Oliveira, L.C., Comas-Rengifo, M.J., 2010.
736 Pliensbachian (Early Jurassic) calcareous nannofossils from the Peniche section (Lusitanian Basin,
737 Portugal): a clue for paleoenviromental recostructions. Marine Micropaleontology 75, 1-16.
738 Reolid, M., Mattioli, E., Nieto, L.M., Rodriguez-Tovar, F.J., 2014. The Early Toarcian Oceanic Anoxic Event
739 in the External Subbetic (South iberian Paleomargin, Westernmost Tethys): geochemistry,
740 nannofossils and ichnology. Palaeogeography, Palaeoclimatology, Palaeoecolology 411, 79-94.

741 Röhl, H.-J., Schmid-Röhl, A., Oschmann, W., Frimmel, A., Schwark, L., 2001. The Posidonia Shale (Lower
742 Toarcian) of SW-Germany: an oxygen-depleted ecosystem controlled by sea level and palaeoclimate.
743 Palaeogeography, Palaeoclimatology, Palaeoecology 165, 27–52.
744 Roth P.H., 1983. Jurassic and Lower Cretaceous calcareous nannofossil in the Western North Atlantic (Site
745 534): biostratigraphy, preservation and some observations on biogeography and paleoceanography.
746 Initial Reports DSDP 76, 587 – 621.
747 Roth, P.H., Thierstein, H., 1972. Calcareous nannoplankton: leg 14 of the DeepSea Drilling Project. In: Hayes,
748 D.E., Pimm, A.C., et al. (Eds.), Initial Reports of the DeepSea Drilling Project 14, 421-485.
749 Saelen, G., Doyle, P., Talbot, M.R., 1996. Stable isotope analyses of belemnite rostra from the Whitby
750 Mudstone Fm., England: surface water conditions during deposition of a marine black shale. Palaios
751 11, 97–117.
752 Sandoval, J., Markus, B., Aguado, R., O' Dogherty, L., Rivas, P., Morard, A., Guex J., 2012. The Toarcian in
753 the Subbetic basin (southern Spain): Bio-events (ammonite and calcareous nannofossils) and
754 carbonate-isotope stratigraphy. Palaeogeography, Palaeoclimatology, Palaeoecolology 342-343, 40-
755 62.
756 Scheck, M., Bayer, U., 1999. Evolution of the Northeast German Basin - inferences from a 3D structural model
757 and subsidence analysis. Tectonophysics 313, 1-2, 145-169.
758 Scheck-Wenderoth, M. P., Krzywiec, P. I., Zühlke, R., Maystrenko, Y., Froitzheim, N., 2008. Permian to
759 Cretaceous tectonics. The geology of central Europe 2, 999-1030.
760 Schmid-Röhl, A., Röhl, J., Oschmann, W., Frimmel, A., Schwark, L., 2002. Palaeoenvironmental
761 reconstruction of Lower Toarcian epicontinental black shales (Posidonia Shale, SW-Germany): global
762 versus regional control. Geobios 35, 13–20.
763 Seilacher, A., 1970. Begriff und Bedeutung der Fossil-Lagerstätten. Neues Jahrbuch für Geologie und
764 Paläontologie, Monatshefte, 34-39.
765 Seilacher, A., Reif, W. E., Westphal, F., 1985. Sedimentological, ecological, and temporal patterns of
766 Fossil-Lagerstätten. Philosophical Transactions of the Royal Society of London B 311, 5–24.

767 Senglaub, Y., Littke, R., Brix, M.R., 2006. Numerical modelling of burial and temperature history as an
768 approach for an alternative interpretation of the Bramsche anomaly, Lower Saxony Basin.
769 International Journal of Earth Sciences 95, 204-224.
770 Suan, G., Pittet, B., Bour, I., Mattioli, E., Duarte, L.V., Maillot, S., 2008. Duration of the Early Toarcian carbon
771 isotope excursion deduced from spectral analysis: Consequence for its possible causes. Earth and
772 Planetary Science Letters 267, 666-679.
773 Suan, G., Mattioli, E., Pittet, B., Lécuyer, C., Suchéras-Marx, B., Duarte L.V., Philippe, M., Reggiani, L.,
774 Martineau, F., 2010. Secular environmental precursors to Early Toarcian (Jurassic) extreme climate
775 changes. Earth and Planetary Science Letters 290, 448-458.
776 Schouten, S., van Kaam-Peters, H.M.E., Rijpstra, W.I.C., Schoell, A. Frimmel et al. 2004. Chemical Geology
777 206, 199-230.
778 Tremolada F., van de Schootbrugge B.V., Erba E., 2005. Early Jurassic schizosphaerellid crisis in Cantabria,
779 Spain: implications for calcification rates and phytoplankton evolution across the Toarcian oceanic
780 anoxic event. Paleoceanography 20, PA2011.
781 van de Schootbrugge, B., McArthur, J.M., Bailey, T.R., Rosenthal, Y., Wright, J.D., Miller, K.G., 2005.
782 Toarcian oceanic anoxic event: an assessment of global causes using belemnite C isotope records.
783 Paleoceanography 20, 1–10.
784 van de Schootbrugge, B., Richoz, S., Pross, J., Luppold, F.W., Hunze, S., Wonik, T., Blau, J., Meister, C., van
785 de Meijst, C. M. H., Suan, G., Fraguas, A., Fiebig, J., Herrle, J.O., Guex, J., Little, C.T.S., Wignall,
786 P.B., Püttmann, W., Oschmann W., 2019. The Schandelah Scientific Drilling Project: A 25-million
787 year record of Early Jurassic palaeoenvironmental change from northern Germany. Newsletters on
788 Stratigraphy 52, 3, 249-296.
789 Visentin, S., Faucher, G., Mattioli, E., Erba E., 2021. Taxonomic revision of genus *Carinolithus*: (Early-
790 Middle Jurassic) based on morphometric analyses and diagenesis observations: Implications for
791 biostratigraphy and evolutionary trends. Marine Micropaleontology 162, 101950.
792 Weitschat, W., 1973. Stratigraphie und Ammoniten des höheren Untertoarcium (oberer Lias epsilon) von NW-
793 Deutschland. Schweiterbartsche Verlagsbuchhandlung, Hannover, Stuttgart, 81 p.

Ziegler, P.A., 1982. Faulting and graben formation in western and central Europe. Philosophical Transactions of the Royal Society 305, 1489.

Ziegler, P.A., 1990. Collision related intra-plate compression deformations in Western and Central Europe. Journal of Geodynamics 11, 357-388.

12. Figure and Table Captions

Fig. 1 – (A) Paleogeographic reconstruction of the North German Basin during the early Toarcian. After Bassoullet et al. (1993). (B) Paleogeographic map of early Toarcian continental shelf area between Baltica and Laurentia showing the location of the study area. CM: Central Massif; RM: Rhenish Massif; AM: Amorikan Massif; LBM: London-Brabant Massif; BM: Bohemian Massif; VS: Vindelizian Swell; YB: Yorkshire Basin; NWGB: North-West German Basin; SWGB: South-West German Basin; PB: Paris Basin; C: Chalhac. Modified from Ziegler (1982).

Fig. 2 – Location map of the investigated cores. (A) Map of Germany with Hildesheim and Braunschweig, the largest towns in the vicinity of L1 and Schandelah drill sites. (B) Map of the Lower Saxony with the occurrences of Lower Jurassic sediments. Locations of the L1 and Schandelah drill sites are indicated. Location map is modified from van de Schootbrugge et al. (2019).

Fig. 3 – Lithostratigraphy, ammonite stratigraphy, calcareous nannofossil biostratigraphy, calcium carbonate content and δ^{13}_{org} curve of the L1 Core. Zonal marker in red.

Fig. 4 - Lithostratigraphy, ammonite stratigraphy, calcareous nannofossil biostratigraphy, calcium carbonate content and $\delta^{13}C_{org}$ curve of the Schandelah Core. Zonal markers in red. Events as detected by van de Schootbrugge et al. (2019) are reported in green.

Fig. 5 - Vertical distribution of taxa in the uppermost Pliensbachian - lower Toarcian interval of the L1 Core. Quantitative abundance of each taxon (x) is obtained with the following classification established in this work for the first time: CA (common to abundant): more than 150 out of 300 specimens ($x > 50\%$ of nannofossil assemblages); C (common): between 51 and 150 out of 300 specimens ($16.7\% < x \leq 50\%$ of nannofossil assemblages); FC (few to common): between 11 and 50 out of 300 specimens ($3.3\% < x \leq 16.7\%$ of nannofossil assemblages); F (few): between 6 and 10 out of 300 specimens ($1.7\% < x \leq 3.3\%$ of nannofossil assemblages); RF (rare to few): between 2 and 5 out of 300 specimens ($0.7\% < x \leq 1.7\%$ of nannofossil assemblages); R (rare): 1 out 300 specimens (0.3% of nannofossil assemblages); RR (extremely rare): not detected within the

300-specimen counting but exclusively in the additional 1000 fields of view (x < 0.3% of nannofossil assemblages).

Fig. 6 - Vertical distribution of taxa in the uppermost Pliensbachian - upper Toarcian interval of the Schandelah Core. The legend adopted for the L1 Core is applied also for the Schandelah Core.

Fig. 7 – Comparison between calcareous nannofossil events recognized in the L1 (B) and Schandelah cores (C) and the biozonation of Bown and Cooper (1998) (A). Zonal markers are in red. The grey band represents the T-OAE defined based on the C isotopic anomaly.

Fig. 8 - Abundances of *S. punctulata*, "small" *S. punctulata* and *L. hauffii* across the Schandelah and L1 cores for the interval in which the 300-specimen counting is performed. Number of specimens detected out of 300 determinable nannofossils are reported against core depth (meters). *Schizosphaerella* crisis and recovery together with *L. hauffii* acme are reported. The position of the T-OAE is also provided in accordance with the C isotopic anomaly.

Fig. 9 - A) Calcareous nannofossil events detected prior and during the T-OAE, plotted against the $\delta^{13}C_{org}$ isotope generalized curve. The lower Toarcian is subdivided into 6 intervals as follows: lowermost Toarcian recovery following the negative excursion at the Pliensbachian/Toarcian boundary (sub-interval a); pre T-OAE anomaly (sub-interval b); rapid decrease (sub-interval c); minimum (sub-interval d); recovery (sub-interval e) and post T-OAE anomaly (sub-interval f). Numbers refer to investigated sections reported in Tab. 1.

PLATE 1

Scale bars represent 2 μm.

Micrographs 1-2 - *B. dubium*, 1) cross - polarized light, 2) quartz lamina, Schandelah Core 22.5 mbsf.

Micrographs 3-4 - *B. finchii*, 3) cross - polarized light, 4) quartz lamina, L1 Core 24.5 mbsf.

Micrographs 5-6 - "large" *B. finchii*, 5) cross - polarized light, 6) quartz lamina, L1 Core 24.9 mbsf.

Micrographs 7-8 - *B. grande*, 7) cross - polarized light, 8) quartz lamina, L1 Core 24.1 mbsf.

Micrographs 9-10 - *B. intermedium*, 9) cross - polarized light, 10) quartz lamina, L1 Core 22.85 mbsf.

Micrographs 11-12 - *Calyculus* spp., 11) cross - polarized light, 12) quartz lamina, L1 Core 23.75 mbsf.

Micrographs 13-14 - *C. superbus crassus*, 13) cross - polarized light, 14) quartz lamina, L1 Core 19.2 mbsf.

Micrographs 15-16 - *C. superbus superbus*, 15) cross-polarized light, 16) quartz lamina, Schandelah Core 26 mbsf.

Micrographs 17-18 - *C. cantabriensis*, 17) cross-polarized light, 18) quartz lamina, L1 Core 24.5 mbsf.

Micrographs 19-20 - *C. crassus*, 21) cross-polarized light, 22) quartz lamina, L1 Core 21.0 mbsf.

Micrographs 21-22 - *C. crucifer*, 23) cross-polarized light, 24) quartz lamina, Schandelah Core 39 mbsf.

Micrographs 23-24 - *C. granulatus*, 25) cross-polarized light, 26) quartz lamina, L1 Core 24.9 mbsf.

Micrographs 25-26 - *C. impontus*, 19) cross-polarized light, 20) quartz lamina, L1 Core 21.2 mbsf.

Micrographs 27-28 - *D. criotus*, 27) cross-polarized light, 28) quartz lamina, Schandelah Core 19.5 mbsf.

Micrographs 29-30 - *D. ignotus*, 29) cross-polarized light, 30) quartz lamina, Schandelah Core 22.5 mbsf.

PLATE 2

Scale bars represent 2 µm.

Micrographs 1-2 - *D. striatus*, 1) cross-polarized light, 2) quartz lamina, Schandelah Core 27.5 mbsf.

Micrographs 3-4 - *L. barozii*, 3) cross-polarized light, 4) quartz lamina, Schandelah Core 22.5 mbsf.

Micrographs 5-6 - *L. crucicentralis*, 5) cross-polarized light, 6) quartz lamina, L1 Core 19.9 mbsf.

Micrographs 7-8 - *L. frodoi*, 7) cross-polarized light, 8) quartz lamina, L1 Core 22.65 mbsf.

Micrographs 9-10 - *L. hauffii*, 9) cross-polarized light, 10) quartz lamina, Schandelah Core 25.0 mbsf.

Micrographs 11-12 - *L. sigillatus*, 11) cross-polarized light, 12) quartz lamina, L1 Core 21.85 mbsf.

Micrographs 13-14 - *L. velatus*, 13) cross-polarized light, 14) quartz lamina, L1 Core 27.5 mbsf.

Micrographs 15-16 - *O. hamiltoniae*, 15) cross-polarized light, 16) quartz lamina, L1 Core 24.9 mbsf.

Micrographs 17-18 - *P. liasicus distinctus* distal view, 17) cross-polarized light, 18) quartz lamina, L1 Core 24.7 mbsf.

Micrographs 19-20 - *P. liasicus distinctus* side view, 19) cross-polarized light, 20) quartz lamina, L1 Core 24.7 mbsf.

Micrographs 21-22 - *S. punctulata*, 21) cross-polarized light, 22) quartz lamina, Schandelah Core 30.0 mbsf.

Micrographs 23-24 - "small" *S. punctulata*, 23) cross-polarized light, 24) quartz lamina, Schandelah Core 30.5 mbsf.

Micrographs 25-26 - *T. patulus*, 25) cross-polarized light, 26) quartz lamina, Schandelah Core 24.5 mbsf.

Micrographs 27-28 - *W. colacicchii*, 27) cross-polarized light, 28) quartz lamina, Schandelah Core 19.5 mbsf.

Micrographs 29-30 - *Watznaueria* sp.1, 29) cross-polarized light, 30) quartz lamina, Schandelah Core 21.0 mbsf

878 **Tab. 1** – Sections considered in Fig. 9 for the calibration of calcareous nannofossil events against the $\delta^{13}C_{org}$

879 isotope curve.